HHS Public Access

Author manuscript

Nature. Author manuscript; available in PMC 2018 May 08.

Published in final edited form as:

Nature. 2017 April 27; 544(7651): 465–470. doi:10.1038/nature22051.

Super-multiplex vibrational imaging

Lu Wei[1], **Zhixing Chen**[1], **Lixue Shi**[1], **Rong Long**[1], **Andrew V. Anzalone**[1], **Luyuan Zhang**[1], **Fanghao Hu**[1], **Rafael Yuste**[2,3,4], **Virginia W. Cornish**[1,2], and **Wei Min**[1,2,4,*]

[1]Department of Chemistry, Columbia University, New York, 10027

[2]NeuroTechnology Center, Columbia University, New York, 10027

[3]Departments of Biological Sciences and Neuroscience, Columbia University, New York, 10027

[4]Kavli Institute for Brain Science, Columbia University, New York, 10032

Abstract

The ability to directly visualize a large number of distinct molecular species inside cells is increasingly essential for understanding complex systems and processes. Even though existing methods have been used successfully to explore structural-functional relationships in nervous systems, profile RNA *in situ*, reveal tumor microenvironment heterogeneity or study dynamic macromolecular assembly[1–4], it remains challenging to image many species with high selectivity and sensitivity under biological conditions. For instance, fluorescence microscopy faces a "color barrier" due to the intrinsically broad (~1500 cm^{-1}) and featureless nature of fluorescence spectra[5] that limits the number of resolvable colors to 2 to 5 (or 7-9 if using complicated instrumentation and analysis)[6–8]. Spontaneous Raman microscopy probes vibrational transitions with much narrower resonances (peak width ~10 cm^{-1}) and thus doesn't suffer this problem, but its feeble signals make many demanding bio-imaging applications impossible. And while surface-enhanced Raman scattering offers remarkable sensitivity and multiplicity, it cannot be readily used to quantitatively image specific molecular targets inside live cells[9]. Here we show that carrying out stimulated Raman scattering under electronic pre-resonance conditions (epr-SRS) enables imaging with exquisite vibrational selectivity and sensitivity (down to 250 nM with 1-ms) in living cells. We also create a palette of triple-bond-conjugated near-infrared dyes that each display a single epr-SRS peak in the cell-silent spectral window, and that with available fluorescent probes give 24 resolvable colors with potential for further expansion. Proof-of-principle experiments on neuronal co-cultures and brain tissues reveal cell-type dependent heterogeneities in DNA and protein metabolism under physiological and pathological conditions, underscoring the potential of this super-multiplex optical imaging approach for untangling intricate interactions in complex biological systems.

*Correspondence and requests for materials should be addressed to wm2256@columbia.edu. Columbia University has filed a patent application based on this work.

Supplementary Information is available in the online version of the paper.

Author Contributions L.W. carried out the spectroscopy, microscopy and biological studies together with L.S. with the help of L.Z., F.H. and R.Y.; Z.C. designed and performed chemical synthesis together with R.L., A.V.A. and L.W. under the guidance of V.W.C. and W.M.; L.W. and W.M. conceived the concept; L.W., Z.C. and W.M. wrote the manuscript with input from all authors.

SRS microscopy, developed for label-free imaging of chemical bonds, uses nonlinear Raman effects to accelerate weak vibrational transition by 10^8 times in the far field (Extended Data Fig. 1) and thereby overcomes the sensitivity or biocompatibility limitations of other Raman imaging modalities[10, 11]. Coupling SRS with strong vibrational tags such as alkynes (C≡C) allows effective imaging of diverse biomolecules[12–15], but detection sensitivity is still limited to about 15 mM for typical chemical bonds such as C-H and 200 μM for the stronger C≡C bond that leaves many targets (such as metabolites, proteins, RNA, organelles) out of reach[10–13].

The sensitivity limits are associated with SRS microscopy having so far always operated in the non-resonance region, with the pump laser energy (ω_{pump}) well below the molecular absorption peak energy (ω_0) (Fig. 1a). Electronic resonance is known to significantly enhance Raman signals[16], and moving from non-resonance ($\omega_0 >> \omega_{pump}$) to rigorous resonance ($\omega_0 = \omega_{pump}$) indeed enhances the detected stimulated Raman loss signal (apparent pump intensity decrease) of IR895 by a factor of about 10^8 compared to the C-O vibrational signal from methanol (cf. purple and yellow spectra in Fig. 1a). But this signal boost comes with a severe sacrifice in chemical specificity: the desired narrow-band vibrational signatures of IR895 are almost overwhelmed by the concurrent broad background that possibly originates from a combination of electronic-resonance four-wave mixing processes and competing pump-probe processes[17].

We hypothesized that judiciously adjusted detuning might retain signal enhancement and improve the contrast between vibrational signal and electronic background. Indeed, a moderate detuning to $\omega_0 - \omega_{pump} \sim 2\Gamma$ (Γ is the homogeneous linewidth, typically ~700 cm^{-1}) results in the electronic pre-resonance SRS (epr-SRS) spectrum of Cy7.5 starting to present an observable peak from the conjugated C=C bonds with a vibrational-signal to electronic-background ratio (S/B) of 0.5 (cf. Fig. 1a, cyan spectrum). Further detuning to ~ 3Γ of ATTO740 gives rise to a clean epr-SRS peak with a vanishing electronic background (cf. Fig. 1a, blue spectrum). A pre-resonance enhancement factor of 2×10^5 can be achieved for this conjugated C=C when compared to C-O in methanol, a magnitude comparable to previous reports for resonance Raman spectroscopy[18]. The epr-SRS detection limit of ATTO740 by targeting this peak is determined to be 250 nM with 1-ms time constant (Fig. 1b). This corresponds to about 30~40 molecules within the focal volume, which is about 1000 times more sensitive than the previous record of non-resonance SRS imaging[12] and comparable to confocal fluorescence microscopy while retaining distinct vibrational contrast.

In our first proof-of-principle epr-SRS microscopy demonstration, we image ATTO740-labeled 5-Ethynyl-2'-deoxyuridine (EdU, a metabolic target for newly synthesized DNA) in HeLa cells with a short pixel dwell time of 4 μs (0.4 s per 320-by-320 frame) (Fig. 1c). The imaging pattern shows high resemblance to the corresponding fluorescence contrast pattern (Extended Data Fig. 2a). Importantly, owing to the narrow vibrational resonance, the epr-SRS signal disappears when the pump laser wavelength λ_{pump} is off resonance by only 2 nm (Fig. 1d)—demonstrating exquisite chemical selectivity unattainable with fluorescence (Extended Data Fig. 3a-d). The epr-SRS signal retains 97% of its initial value even after 100

frames of continuous imaging (Fig. 1e, Extended Data Fig. 2b), indicating satisfying photo-stability in the pre-resonance region.

To demonstrate the versatility of epr-SRS imaging, we imaged the ATTO740 immuno-labeled intracellular proteins (Fig. 1f-g, Extended Data Fig. 2c) alpha-tubulin with clearly resolved tubule structures (Fig. 1f) and Tom20 (a mitochondria receptor, Fig. 1g) and membrane receptors of tumor markers (keratin 18 in Fig. 1h; Extended Data Fig. 2d). In addition to immuno-labeling, epr-SRS imaging of genetically encoded H2B proteins in live cells was also achieved through SNAP-tagging with far-red silicon-Rhodamine (SiR) dye (Fig. 1i). Organelle targets (MitoTracker deep red, Fig. 1j) and chemical drugs (methylene blue, a widely used drug and a photosensitizer in photodynamic therapy, Fig. 1k, likely enriched in lysosomes) can also be visualized in live cells. Finally, to demonstrate utility in a small-molecule based functional assay, we monitored the production of a non-fluorescent indigo product from a classic *lacZ* gene-expression assay in live *E. coli* (Fig. 1l).

We next focused on developing an epr-SRS reporter dye palette. Characterization of 28 commercial dyes across a wide range of ω_0 (Fig. 2a, Extended Data Table 1) confirmed that their Raman scattering cross-sections (σ(C=C)) increase steeply as ω_0 approaches ω_{pump}. This trend can be fitted quantitatively to the Albrecht A-term pre-resonance approximation, using a single fitting parameter K (Eq. 1) (Fig. 2a, red line):

$$\sigma = K\omega_0(\omega_0 - \omega_{vib})^3\left(\frac{(\omega_{pump}^2 + \omega_0^2)}{(\omega_0^2 - \omega_{pump}^2)^2}\right)^2 \quad (1)$$

where ω_{vib} is the vibrational transition energy and K is a collection of frequency-independent factors of the dyes[16, 19]. We thus defined an optimal epr-SRS excitation region as $2\Gamma < \omega_0 - \omega_{pump} < 6\Gamma$ (Fig. 2a, grey shaded) to ensure both chemical specificity (S/B > 0.5) and sensitivity (< 5 μM with 1-ms). Within this near-infrared region approximately between 650 nm and 800 nm, 6 commercial dyes with largely overlapping fluorescence (Extended Data Fig. 3e) but mutually resolvable epr-SRS spectra (Fig. 2b, dash-lined) were identified as multiplexable reporters for the epr-SRS palette.

We then selected 5 C=C peaks to demonstrate the multiplex imaging capability (Fig. 2b, arrowed). Spectral cross-talks are minimized by a linear combination algorithm (see methods). We further noted that the epr-SRS imaging in the near-infrared is orthogonal to fluorescence detection in the visible region (the non-resonance SRS region), so merging epr-SRS and fluorescent palettes enabled imaging with 8 different colors (5 quantitative epr-SRS of C=C bonds and 3 fluorescence channels) of the same set of fixed cells (Fig. 2c, Extended Data Fig. 4). Combining fluorescent proteins in the visible region with commercial organelle trackers in the epr-SRS region also enabled 8-color imaging of live cells (Fig. 2d), a feat difficult to achieve by other means.

The epr-SRS dye palette can be expanded further, especially when going beyond conjugated C=C bonds and targeting triple bonds such as alkynes (C≡C) and nitriles (C≡N) that display

a single sharp Raman peak in the wide silent window (from 1800 to 2800 cm^{-1})[12–15, 20]. The challenge here is that the triple bonds must be coupled with an electronic transition to enable pre-resonance enhancement, which will depend sensitively on the electronic-vibrational coupling strength[16]. Hence, simply installing a triple bond onto an arbitrary position of a dye will most often not yield satisfying signals.

We rationally designed a new library of near-infrared dyes (Fig. 3a), where nitrile or alkyne triple bonds directly participate in the π-conjugation systems of the molecule, with xanthene identified as a privileged scaffold[21,22] after initial screening. To generate more vibrational colors, we employed three combined strategies guided by the classical $\omega_{vib} \propto \sqrt{k/\mu}$ equation where k is the spring constant reflecting the bond strength and $\mu = m_1 m_2/(m_1 + m_2)$ is the reduced mass. As illustrated by the x- and y- axes in Fig. 3a, substituting the 10-position of xanthene from O atom to C and Si[23] (Fig. 3a, green marked), gradually expanding the xanthene rings (Fig. 3a, yellowed marked), and modifying the terminal groups for alkyne dyes (Fig. 3a, purple marked) all fine tune the triple bond strength by affecting the electron-density of the π-conjugation system. As indicated as z-axis, combinatorial isotopic editing of the two atoms involved in the triple bond (Fig. 3a, highlighted in red and blue) enables local modulation of their reduced mass into 4 possible combinations[24] that further expand the vibrational palette.

We synthesized most of the dyes (including their ^{13}C and ^{15}N isotopologues) in our conceived library (Fig. 3a), referring to promising structures with mutually resolvable epr-SRS peaks as MAnhattan Raman Scattering (MARS) dyes. We selected two sets of MARS palettes (selected structures are underlined in Fig. 3a) with up to 14 well-resolved epr-SRS colors in the cell-silent window (Fig. 3b) (Extended Data Table 2), with all dyes displaying satisfying specificity (S/B > 5) and sensitivity (< 5 μM with 1-ms). With the 6 commercial dyes in the fingerprint region, our expanded vibrational palette thus consists of 20 resolvable reporters in the near-infrared. Combining this vibrational palette with 4 more fluorescence channels typically obtainable in the visible region allows us to access 24 colors for optical super-multiplexing.

Our newly developed epr-SRS vibrational palette has biocompatibility that ensures sufficient cell viability (Extended Data Fig. 5), the required photostability (Extended Data Fig. 6) and effective linear unmixing (Extended Data Fig. 7) to enable proof-of-principle imaging on live HeLa cells. After being separately stained with individual dyes and then mixed together, these cells are subjected to 16-color live-cell imaging, which quadruples the number of color channels typically achieved by fluorescence alone. The resultant image shown in Fig. 4a was acquired through sequential imaging in 15 minutes, but further system development should enable simultaneous imaging. We then used this super-multiplexing technique to probe metabolic activity in complex nervous systems consisting of multiple cell types, under either physiological or pathological conditions. First, we used 8-color imaging to image DNA replication and protein synthesis activities, two crucial processes in neural development and function, in hippocampal neuronal cultures (Fig. 4b, Extended Data Fig. 8a) and organotypic cerebellar tissues (Fig. 4c, Extended Data Fig. 8b) and reveal highly heterogeneous DNA synthesis. Confirmed with labeling specificity (Fig. 4b1), we identified two newly divided

cells (EdU^+, Fig. 4b2, arrowed) in neuronal co-cultures. Multicolor cross-examination revealed that one was astrocytic (Fig. 4b3-b4, arrowed, βIII-tubulin$^-$, NeuN$^-$ and Nestin$^+$, GFAP$^+$), while the other oligodendrocytic (Fig. 4b3-b5 double-arrowed, βIII-tubulin$^-$, NeuN$^-$, Nestin$^-$, GFAP$^-$ but MBP$^+$). Moving to imaging of organotypic cerebellar tissues of P11 mice (Fig. 4c1), we observed a high number of EdU^+ cells likely concentrated in the molecular layer (Fig. 4c2), which might be a progenitor-cell niche (Fig. 4c3-c5, Nestin$^+$, MBP$^+$ but NeuN$^-$, highlighted by arrows). These observations establish that our super-multiplex imaging platform is well suited for probing molecular heterogeneity in nervous systems.

We then studied neuronal systems under proteasomal stress. Proteostasis, the balance between new protein synthesis and degradation of aberrant proteins, is precisely regulated through cellular “quality control”, particularly the ubiquitin-proteasome system, with proteasome dysfunction implicated in many neurodegenerative diseases and aging processes[25]. When studying individual cell types under proteasomal stress (modeled by applying proteasome inhibitor MG132), astrocytes were found to be more resistant than neurons and oligodendrocytes[26]. Because such cell-type dependent vulnerability is unexplored in more realistic environments where different cells will co-exist, we used 8-color imaging to study the global proteostasis stress in neuronal co-cultures with largely preserved astrocyte-neuron coupling. As expected, applying MG132 (Fig. 4d1) retarded the proteome turnover (Extended Data Fig. 9). Interestingly, obvious cytosolic proteome aggregations (inclusions) were observed only in the chase channel (Fig. 4d2-d3), suggesting newly synthesized proteins are more susceptible to proteasomal impairment and prone to aggregation. This is consistent with the fact that up to 30% of newly synthesized proteins are misfolded[27]. Most importantly, subsequent cross-channel examination indicated that proteome inclusions appeared mostly in astrocytes instead of neurons (Fig. 4d4-d5, 4e, Supplementary Data). Considering that the formation of protein inclusions may exert a protective role by sequestering potentially harmful species from the cytosol[28], this result suggests that the astrocyte resistance observed before might be due to their ability to actively form protein inclusions that sequester the toxic misfolded species, whereas neurons are unable to do so.

While the above proof-of-principle observations demonstrate already the potential of our technique, it can be improved further along multiple fronts. First, the MARS dye palette can be potentially expanded to 50 or more colors by filling the rather broad cell-silent window with individual sharp peaks from novel vibrational moieties. Second, genetically encoded infrared proteins could also be engineered to serve as vibrational reporters[29]. Third, hyper-spectral imaging[30] can be implemented to realize faster and simultaneous signal acquisition. Given these expected further improvements, and as our technique is offering sensitivity, resolution, labeling compatibility and biocompatibility approaching or similar to that of fluorescence microscopy, we expect it to find wide applications in probing complex systems.

Methods

1. Stimulated Raman scattering (SRS) microscopy

An integrated laser (picoEMERALD with custom modification, Applied Physics & Electronics, Inc) was used as light source for both pump and Stokes beams. Briefly, picoEMERALD provided an output pulse train at 1064 nm with 6-ps pulse width and 80 MHz repetition rate, which served as the Stokes beam. The frequency-doubled beam at 532 nm was used to synchronously seed a picosecond optical parametric oscillator (OPO) to produce a mode-locked pulse train (the idler beam of the OPO was blocked with an interferometric filter) with 5~6 ps pulse width. The wavelength of the OPO was tunable from 720 to 990 nm, which served as the pump beam. The intensity of the 1064 nm Stokes beam was modulated sinusoidally by a built-in electro-optic modulator (EOM) at 8 MHz with a modulation depth of more than 95%. The pump beam was spatially overlapped with the Stokes beam with a dichroic mirror inside picoEMERALD. The temporal overlap between pump and Stokes pulse trains was ensured with a built-in delay stage and optimized by the SRS signal of deuterium oxide (99.9 atom % D, 151882 ALDRICH).

Pump and Stokes beams were coupled into an inverted laser-scanning microscope (FV1200MPE, Olympus) optimized for near IR throughput. A 25X water objective (XLPlan N, 1.05 N.A., MP, Olympus) with both high near IR transmission and large field of view was used for measurements of all solutions, cells and tissues unless specified. A 60X water objective (UPlanAPO/IR, 1.2 N.A., Olympus) with high near IR transmission was used for X-gal assay and live-cell 8-color imaging. The pump/Stokes beam size was matched to fill the back-aperture of the corresponding objectives for imaging. The forward going pump and Stokes beams after passing through the samples were collected in transmission with a high N.A. condenser lens (oil immersion, 1.4 N.A., Olympus), which was aligned following Köhler illumination. A telescope was then used to image the scanning mirrors onto a large area (10 mm by 10 mm) Si photodiode (FDS1010, Thorlabs) to descan beam motion during laser scanning. The photodiode was reverse-biased by 64 V from a DC power supply to increase both the saturation threshold and response bandwidth. A high O.D. bandpass filter (890/220 CARS, Chroma Technology) was used to block the Stokes beam completely and transmit the pump beam only. The output current of the photodiode was electronically pre-filtered by an 8 MHz band-pass filter (KR 2724, KR electronics) to suppress both the 80 MHz laser pulsing and the low-frequency contribution due to laser scanning across the scattering sample. It was then fed into a radio frequency lock-in amplifier (SR844, Stanford Research Systems or HF2LI, Zurich instrument) terminated with 50 Ω to demodulate the stimulated Raman loss signal experienced by the pump beam. The in-phase X-output of the lock-in amplifier was fed back into the analog interface box (FV10-ANALOG) of the microscope.

All laser powers were measured after objective lens. For spectroscopy measurement in Fig. 1, P_{Stokes}=18.4 mW. For detection sensitivity measurement, laser powers were P_{pump}=24 mW, P_{Stokes}=184 mW. For cellular and tissue imaging, the range of laser powers used were P_{pump}= 7~24 mW, P_{Stokes}= 46~120 mW. Pixel dwell times for all images were ranging from the fastest 4 μs (0.4 s per 320-by-320 frame, Fig. 1c-e) to the slowest 200 μs (20.5 s per 320-

by-320 frame, Fig. 2c-d, Fig. 4b-d). Time constants of lock-in amplifier were chosen to be about two times shorter than the pixel dwell time. All fluorescence images were acquired by commercial Olympus FV1200MPE microscope equipped with 488nm, 543nm and 633nm CW lasers. Two-photon fluorescence was excited by the tunable pump laser at designated wavelengths and detected by Non-descanned PMTs. For two-photon fluorescence imaging of Nucblue (Figs. 2 and 4), it is excited by OPO laser at 780 nm, and the fluorescence was detected after passing through a 690 nm short pass filter, a 570 nm short pass dichroic and a 450/40 nm band-pass filter (Thorlabs, FB450-40). The detections for two-photon fluorescence signals of Nucblue in the UV/blue and of epr-SRS in the near IR are still orthogonal to each other with no issue of signal overlapping. For two-photon fluorescence imaging of Alexa647 (Extended Data Fig. 3c, d), it is excited by OPO laser around 810 nm, and the fluorescence was detected after passing through a 690 nm short pass filter, a 570 nm short pass dichroic.

2. Stimulated Raman scattering (SRS) spectra acquisition

Stimulated Raman scattering spectra for all dyes were acquired by fixing the Stokes beam at 1064 nm, and scanning the pump beam through the designated wavelength range point by point.

3. Linear combination algorithm

Since epr-SRS signals are linearly dependent on analyte concentrations, quantitatively distinguishing different dyes with overlapped Raman bands could be performed through a simple and robust linear combination algorithm. The measured N-channel epr-SRS signals (***S***) for N dyes could be expressed as the products of a N×N dye Raman cross-section matrix (***M***) and dye concentrations (***C***), with addition of the cellular amide backgrounds in each channels (***B***):

$$S=M\cdot C+B$$

Dye concentrations were thus solved by:

$$C=M^{-1}\cdot(S-B)$$

$$C=\begin{bmatrix} C_{dye1} \\ \vdots \\ C_{dyeN} \end{bmatrix};\ S=\begin{bmatrix} S_{channel1} \\ \vdots \\ S_{channelN} \end{bmatrix};\ B=\begin{bmatrix} B_{channel1} \\ \vdots \\ B_{channelN} \end{bmatrix};\ M=\begin{bmatrix} \sigma_{dye1,\ channel1} & \cdots & \sigma_{dye5,\ channel1} \\ \vdots & \vdots\cdots & \vdots \\ \sigma_{dye1,\ channelN} & \cdots & \sigma_{dye5,\ channelN} \end{bmatrix}$$

For Fig. 2c-d of epr-SRS in fingerprint region, ***B*** was achieved by acquiring a reference image at the label-free channel of 2940 cm^{-1} for total proteins and then scaling it as backgrounds at individual epr-SRS channels. The scaling factors were determined in reference HeLa cells without labels under the corresponding imaging conditions. For Fig. 4 with MARS dyes, ***B*** was vanishing and the equation becomes:

$$C = M^{-1} \cdot S$$

The algorithm was implemented by a *Matlab* program.

4. Protein labeling with dye NHS esters

1) Conjugation to secondary antibodies—Dye NHS esters were dissolved in DMSO to a concentration of 2 mg/mL. Secondary antibodies were dissolved/diluted to 2mg/mL in PBS buffer of a pH of 8.3, adjusted with sodium bicarbonate buffer. For antibodies purchased with concentrations lower than 2 mg/mL, proteins were first concentrated with Amicon® Ultra Centrifugal Filters (UFC501096, EMD, Millipore). A 50 μL dye-NHS solution was slowly added to a 0.5 mL protein solution. Reaction was incubated at RT for 60 min under constant but slow stirring. The labeled proteins could be separated from unreacted dye NHS esters by gel permeation chromatography with Sephadex™ G-25 (G25150 SIGMA) with a column of diameter around 1 cm and length longer than 12 cm. Sephadex® G-25 was first swelled in PBS buffer at 90 °C water bath for 1 h. After gel settling down in room temperature, buffer was exchange to fresh PBS buffer and gels were stored at 4 °C. For gel chromatography, column was packed with swelled gels, and then equilibriumed with PBS. The labeled protein solution was then loaded and eluted with PBS buffer. First band with light color for dye conjugated proteins was collected. This solution was then centrifuged and supernatant was collected and concentrated with Amicon® Ultra Centrifugal Filters (UFC501096, EMD, Millipore) into a final concentration of 1 - 2 mg/mL in PBS with 30% glycerol and 5 mM sodium azide and stored at -20 °C.

2) Conjugation to Wheat Germ Agglutinin (WGA, L0636 SIGMA)—All procedures were the same as described above except the dye-protein ratio: a 17.5 μL 2 mg/ml dye-NHS solution was slowly added to a 0.5 mL 2mg/ml WGA solution.

5. Sample information (cell, tissues, antibodies and chemical reagents)

All samples were made into imaging chambers using an imaging spacer (GBL654008 SIGMA) between a coverslip and a microscope slide. The chamber was filled with PBS for imaging. All imaging results were experimentally replicated for more than 5 times.

Cell lines—Cell lines were purchased from ATCC: HeLa (ATCC® CCL-2™); MCF7 (ATCC® HTB-22™); HEK 293T/17 (ATCC® CRL-11268™). These cell lines were authenticated and mycoplasma negative. Cell medium: DMEM medium was made of 90% DMEM (11965, invitrogen), 10% FBS (10082, invitrogen) and 1X penicillin/streptomycin (15140, invitrogen). Methionine-deficient DMEM medium was made by supplying 4 mM L-glutamine, 0.2 mM L-cystine, 10% FBS and 1% penicillin/streptomycin to DMEM without L-methionine, L-cysteine and L-glutamine (D0422 SIGMA).

Mice and tissues—The animal experimental protocol (AC-AAAQ2457) was approved by the Institutional Animal Care and Use Committee at Columbia University. 400 μm thick cerebellar brain slices from P11 wild-type (C57BL/6) mice of either sex were cultured with Methionine-deficient brain slice culture medium containing 1 mM AHA and 100 μM EdU

for 17 h. Organotypic slices were then fixed with 4% PFA for 30 min, followed with 0.5% Triton permeabilization for overnight at 4 °C. No statistical method was used to predetermine sample size. All experimental procedures were performed in a non-blinded manner and no randomization was applied.

Antibodies: Primary antibodies for single-color labeling: Anti-Fibrillarin antibody - Nucleolar Marker in rabbit (ab5821,Abcam); Anti-200 kD Neurofilament Heavy antibody in rabbit (ab8135, Abcam); Anti-α-Tubulin antibody in rabbit (ab18251, Abcam); Anti-Tom20 Antibody in rabbit (sc-11415, Santa Cruz Biotechnology); Anti-Giantin antibody in rabbit (ab24586, Abcam); Anti-Cytokeratin 18 antibody in mouse (ab7797, Abcam); Anti-CD44 antibody in mouse (ab6124, Abcam); Anti-EpCAM antibody in rabbit (ab71916, Abcam); Anti-IGF1 Receptor beta subunit antibody in mouse (ab80547, Abcam). For multicolor labeling: Anti-Fibrillarin antibody - Nucleolar Marker in mouse (ab4566, Abcam); Anti-α-Tubulin antibody in chicken (ab89984, Abcam); Anti-Giantin antibody in rabbit (ab24586, Abcam); Anti-βIII-tubulin in chicken (ab107216, Abcam); Anti-Myelin Basic protein in mouse (ab62631, Abcam); Anti-GFAP in goat (ab53554, Abcam); Anti-Nestin in rat (ab81462, Abcam); Anti-NeuN in rabbit (ab177487, Abcam). Secondary antibodies: Goat-anti-rabbit ATTO740 antibody (49559, Sigma); Goat-anti-mouse ATTO740 antibody (2111, Hypermol); Goat-anti-rabbit ATTO700 antibody (2310, Hypermol); Goat anti-chicken CF640R antibody (20084, Biotium); Donkey-anti-rabbit Alexa568 (ab175692, Abcam); Donkey-anti-rat Alexa488 (ab150153, Abcam). Donkey-anti-mouse antibody (Sigma, SAB3701101), Donkey-anti-chicken (Invitrogen, SA172002) and Donkey-anti-goat antibody (Sigma, G6638) were conjugated with MARS dyes.

Fluorophores: ATTO740 NHS ester (59808 SIGMA), IR895 (392375 SIGMA). More dyes are listed in Extended Data Table 1.

6. Experimental procedures for epr-SRS imaging

Imaging newly synthesized DNA in HeLa cells by metabolic incorporation of 5-Ethynyl-2′-deoxyuridine (EdU, T511285, Aldrich) and detection with ATTO740-azide (Fig. 1c-e, Extended Data Fig. 2a-b)—HeLa cells were seeded on a coverslip in a petri-dish with DMEM for 20 h, then replaced with DMEM medium without FBS for another 20 h for synchronization. 10 μM EdU in fresh DMEM medium were then added to cells for 15 h. Cell were fixed with 4% PFA for 20 min, permealized with 0.5% Triton permeabilization for 10 min. 1 μM ATTO740-azide (AD 740-101, ATTO-TEC) in Click-iT® Cell Reaction Buffer (C10269, Invitrogen) was then added to cells to react with EdU for 20 min. Cells were washed twice with PBS before imaging.

Immuno-staining for single-color epr-SRS imaging of fixed HeLa or MCF7 cells (Fig. 1f-h, Extended Data Fig. 2c-d)—HeLa/MCF7 cells were seeded on a coverslip in a petri-dish with 2 mL of DMEM for 20 h, and then fixed with 4% PFA for 20 min or methanol for 25 min. After fixation, cells were washed with 10% goat serum/1% BSA/0.3M glycine solution twice before permeabilization in 0.1% Tween PBS for 40 min. Primary antibody was subsequently added by 1:200 dilution in 3% BSA at 4 °C overnight. After blocking with 10% goat serum for 30 min, secondary antibody conjugated with

fluorophores was added by 1:100 dilution in 10% goat serum at 4 °C overnight. The samples were blocked with 10% goat serum for 30 min before imaging.

Epr-SRS imaging of SiR-SNAP-tagged H2B proteins (Fig. 1i)—HEK293T cells were seeded on a coverslip in a petri-dish with DMEM for 20 h before transfected with 250 ng SNAP-H2B plasmid (New England BioLabs) for 48 h. 10 μM SNAP-SiR (S9102S, New England BioLabs) were then added to medium for 45 min at 37 °C. Cells were washed 3 times with PBS before imaging.

Epr-SRS imaging of Mitotracker deep red (Fig. 1j)—500 nM MitoTracker deep red (M22426, Invitrogen) in HBSS was added to cells for 20 min at 37 °C. Cells were washed twice with PBS before imaging.

Epr-SRS imaging of methylene blue (Fig. 1k)—10 μM methylene blue (M9140 SIGMA-ALDRICH) in PBS was added to cells for 20 min at 37 °C. Cells were washed twice with PBS before imaging.

Epr-SRS imaging of the indigo product from X-gal gene expression assay (Fig. 1l)—BL21 E. Coli were grown in LB to log phase before adding 100 μM X-gal (XGAL-RO ROCHE) and 1 mM IPTG (I6758 SIGMA-ALDRICH) for 20 min at 37 °C. E. Coli were then concentrated and washed with PBS before imaging.

8-color epr-SRS and fluorescence imaging of fixed HeLa cells (Fig. 2c)—HeLa cells were seeded on a coverslip in a petri-dish with DMEM for 20 h, then replaced with methionine-deficient DMEM medium for 30 min. 1 mM L-Azidohomoalanine (AHA, C10102, Invitrogen) and 100 μM EdU were then added into medium for 18 h. 400 nM MitoTracker® Orange CMTMRos (M-7510, Invitrogen) was added into medium for 30 min and 2 μM Alexa 488-WGA (W11261, Invitrogen) was added together for the last 15 min before fixation of the cells with 4% PFA for 8 min followed with methanol for 20 min. The following immuno-staining procedures were same as described above. After secondary-antibody incubation, samples were blocked with 10% goat serum for 30 min. Then 5 μM Cy5.5-azide (178, AAT-Bioquest) with Click-iT® Cell Reaction Buffer was added to cells to react with EdU for 20 min. After washing with PBS, 2.5 μM Alexa 647-alkyne (A10278, Invitrogen) with Click-iT® Cell Reaction Buffer was added to cells to react with AHA for 20 min. Lastly, NucBlue® Fixed Cell ReadyProbes® Reagent (R37606, Invitrogen) was added to cells for 10 min. Cells were washed with PBS before imaging.

8-color epr-SRS and fluorescence imaging of live HeLa cells (Fig. 2d)—HeLa cells were first seeded on coverslips in petri dishes with DMEM culture medium at 37 °C for 24 h. ER-GFP (C10590, Invitrogen) and Actin-RFP (C10583, Invitrogen) plasmids were transfected into cells for 48 h following the protocol from Invitrogen. 500 μM oleic acid (O1383 SIGMA) coupled with BSA in DMEM culture medium was then added to cells for 7 h to induce the formation of lipid droplets. Before imaging, cells were first incubated with 6 μM SYTO60 (S11342, Invitrogen), 120 nM LysoTracker Deep Red (L12492, Invitrogen) and 400 nM Rhodamine 800 (83701 SIGMA) in HBSS simultaneously for 30 min at 37 °C, followed by staining with NucBlue® Live ReadyProbes® Reagent (R37605, Invitrogen) in

HBSS for 20 min at 37 °C. Then cells were incubated with ATTO 740-conjugated WGA in HBSS for 30 min at 37 °C, followed by staining with LipidTOX Deep Red (H34477, Invitrogen) in HBSS with a dilution of 1:20 for 30 min at room temperature before imaging.

16-color epr-SRS and fluorescence imaging of live HeLa cells (Fig. 4a)—HeLa cells were first seeded in 24-well dish for 20 h. Each well of cells were labeled with a single color of epr-SRS or fluorescent dyes for 30 min in PBS: MARS2237 (1 μM), MARS2228 (4 μM), MARS2209 (1 μM), MARS2200 (4 μM), MARS2183 (1 μM), MARS2176 (4 μM), MARS2154 (1 μM), MARS2147 (4 μM), ATTO OXA12 (10 μM), Cy5.5 (2 μM), MitoTracker deep red (2.5 μM), SYTO60 (10 μM). FM 4-64 (T13320, Invitrogen, 20 μg/ml), MitoTracker orange (M7510, Invitrogen, 400 nM), Alexa488-WGA (W11261, Invitrogen, 2 μg/ml), Nucblue (R37605, Invitrogen). Cells were then washed with PBS and detached from each well by trypsin treatment for 2 min; then mixed together in fresh DMEM medium before gently centrifuge (1000 rpm, 1.5 min) to pellet. PBS was added to the pellet and after gentle mix, cells were sandwiched in imaging chamber. After settling down for 15-20 min on imaging stage to reduce cell movement, images were acquired. Single dye staining and 2-color mix were first examined and no cross staining between cells was found during the imaging period (i.e. each cell was maintained with a single pre-stained color). We did not observe obvious stage drift during 16-color image acquisitions. Fig. 4a was acquired through sequential imaging in 15 minutes.

8-color epr-SRS and fluorescence imaging of hippocampal neuronal cultures and cerebellar brain slices (Fig. 4b-c)—Regular hippocampal neuron medium was made of Neurobasal A Medium (10888, Invitrogen), 1× B27 serum free supplement (17504, Invitrogen) and 0.5 mM glutamine (25030, Invitrogen). Methionine-deficient neuron medium was custom made from regular recipe of Neurobasal A medium (10888, Invitrogen) without methionine, and supplied with 1× B27 serum free supplement and 0.5 mM glutamine. Methionine-deficient medium for organotypic cerebellar brain slices was made by supplying methionine-deficient neuron medium with 1× B27 serum free supplement, 2 mM glutamine, 0.5% glucose and 1% penicillin/streptomycin.

Regular medium in D9 hippocampal neuronal cultures was first replaced by methionine-deficient medium containing 1 mM AHA and 100 μM EdU for 17 h. Cells were then fixed with 4% PFA for 20 min, followed with 0.5% Triton permeabilization for 15 min. Primary antibodies were then simultaneously added with 1:120 dilution in 3% BSA for overnight at 4 °C. After blocking with 10% donkey serum for 30 min, secondary antibodies conjugated with fluorophores were added with 1:80 dilution in 10% donkey serum for overnight at 4 °C. Samples were blocked with 10% donkey serum for 30 min with NucBlue® Fixed Cell ReadyProbes® Reagent added for the last 10 min. Then 1 μM MARS2228-azide with Click-iT® Cell Reaction Buffer was added to cells/slices to react with EdU for 20 min. After washing with PBS, 12 μM Alexa 647-alkyne with Click-iT® Cell Reaction Buffer was added to react with AHA for 20 min. Cells were washed with PBS before imaging.

8-color epr-SRS and fluorescence imaging in neuronal cultures (Fig. 4d)—Regular Medium of D12 hippocampal neuronal cultures was replaced by methionine-deficient medium containing 1mM L-Homopropargylglycine (HPG, C10186, Invitrogen) for

12 h. The medium was then exchanged to fresh methionine-deficient medium containing 1mM AHA with or without 10 μM MG132 (M7449 SIGMA) for another 10 h. Cells were fixed with 4% PFA for 20 min, permeabilized with 0.5% Triton for 15 min. The immuno-staining procedures were the same as described above. Then 1.25 μM MARS2228-azide with Click-iT® Cell Reaction Buffer was added to cells/slices to react with HPG for 20 min. After washing with PBS, 4 μM Alexa 647-alkyne with Click-iT® Cell Reaction Buffer was added to react with AHA for 20 min. Cells were washed with PBS before imaging.

Image statistics for Fig. 4e: 6 technical replicates of 8-colour images were acquired from 3 independent neuronal co-cultures (the same condition as described above for Fig. 4d) for statistical presentation. For each neuronal co-culture, 2 fields of view were selected close to the center of the culture dish to maintain consistency. All images were taken under the same imaging parameters. Cross-checking 8-colour staining, the percentages of astrocytes with aggregations (i.e., the number of astrocytes with aggregations divided by the total number of astrocytes) and the percentages of neurons with aggregations (i.e., the number of neurons with aggregations divided by the total number of neurons) were calculated for each image sets. Their means and standard deviations are then presented in Fig. 4e, together with a P value from two-sided Student's t-test. Refer to Supplementary Data for source data.

Live/dead cell viability assay (Extended Data Fig. 5.)—It is performed using the LIVE/DEAD viability/cytotoxicity kit for mammalian cells (Molecular Probes L-3224). HeLa cell standards and HeLa cells with dye staining or SRS pre-exposure were incubated with 2 μM calcein AM and 4 μM EthD-1 working solution for 20 minutes at 37 °C before imaging.

Data and code availability: All data supporting this study are available from the corresponding author on request.

Extended Data

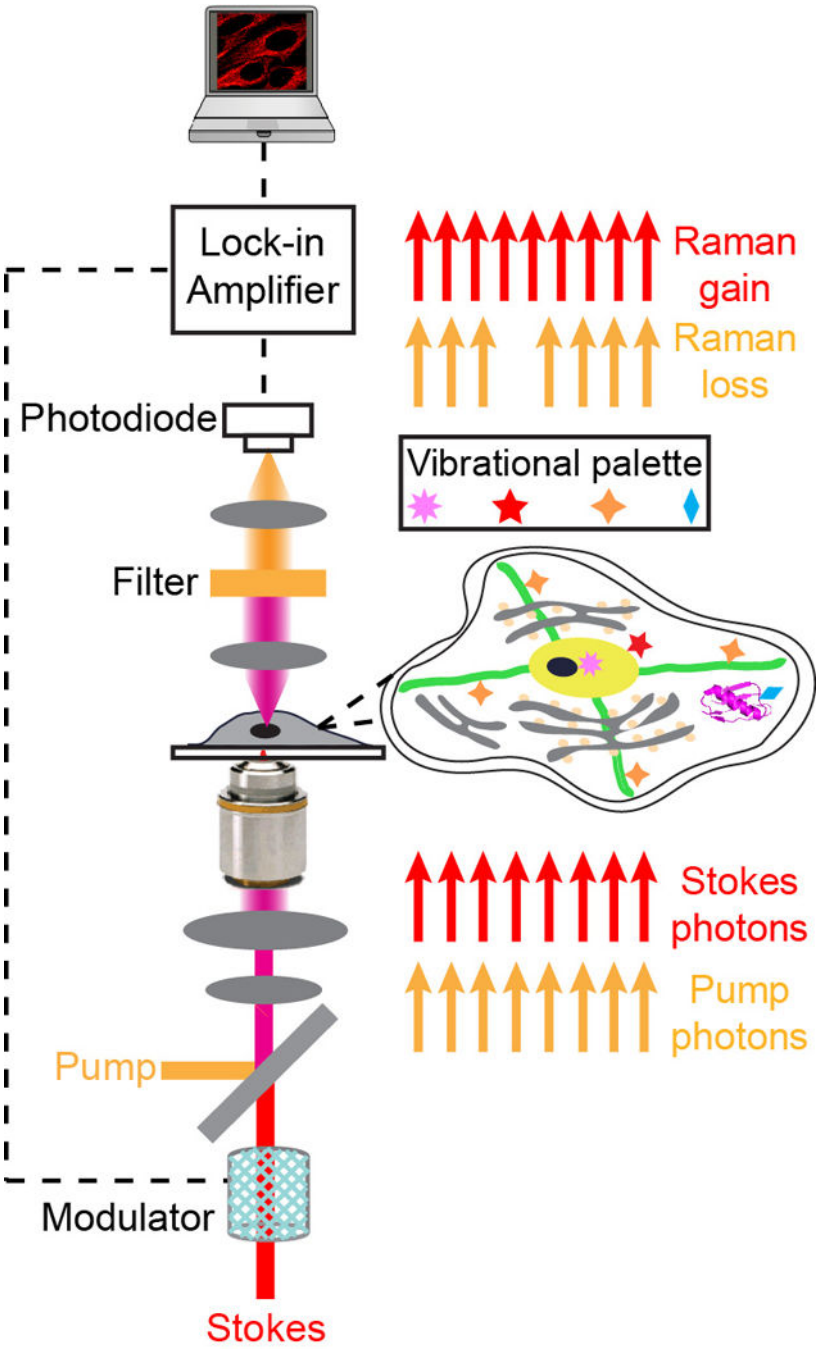

Extended Data Fig. 1. Apparatus of SRS microscopy

A narrow-band pump laser (6-ps pulse width) and an intensity modulated Stokes laser (fixed at 1064 nm, 6-ps pulse width) are both temporally and spatially synchronized before collinearly focused onto cells samples. When the energy difference between the pump photons and the Stokes photons matches with the vibrational frequency (ω_{vib}) of the targeted chemical bonds, the chemical bonds are efficiently excited to the vibrational excited state.

For each transition, a photon in the pump beam is annihilated (stimulated Raman loss) and a photon in the Stokes beam is created (stimulated Raman gain). A lock-in detection scheme is used to sensitively measure the intensity loss of the pump beam (i.e. stimulated Raman loss).

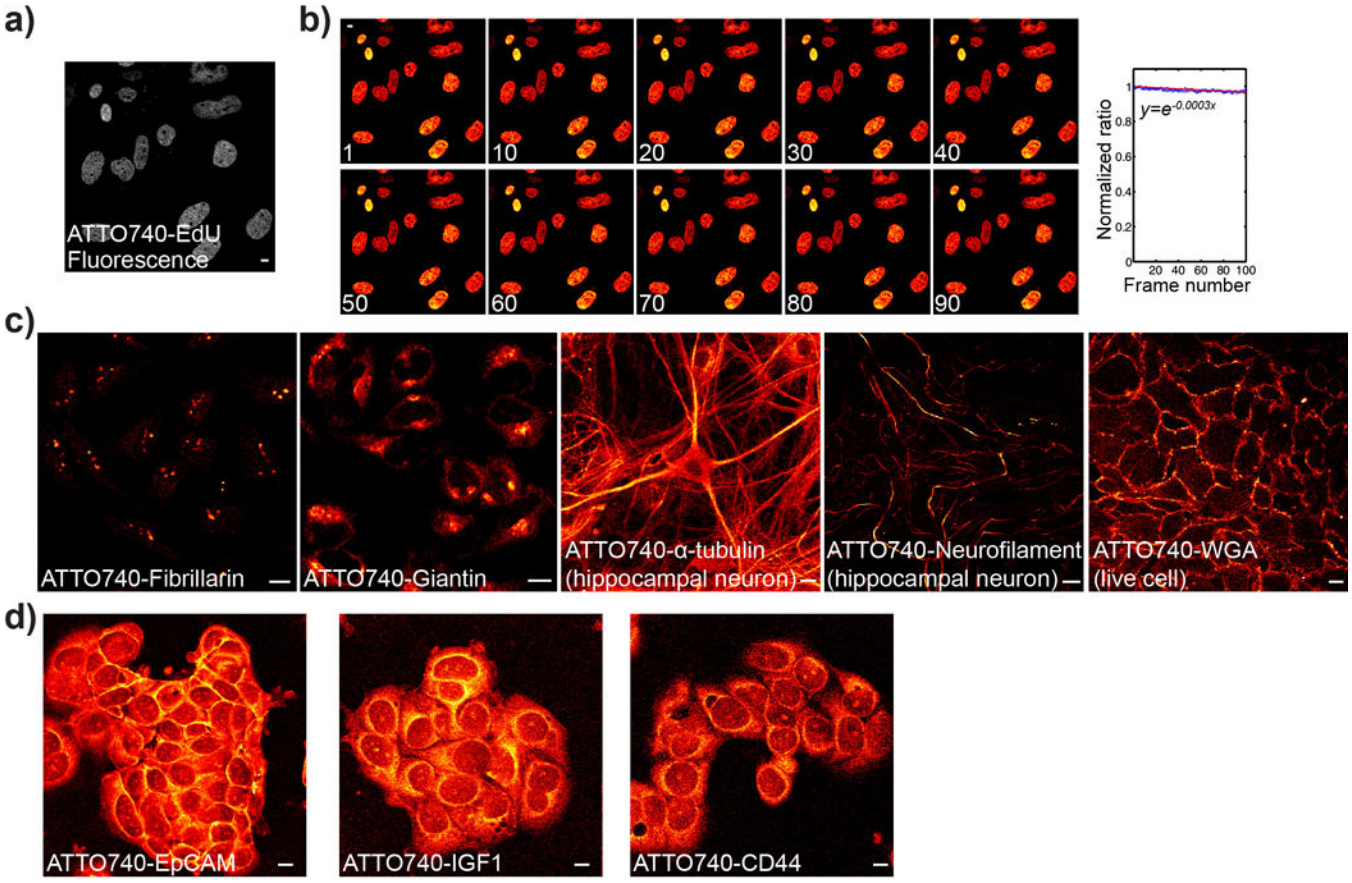

Extended Data Fig. 2. Sensitive epr-SRS imaging of ATTO740 labeled individual targets in HeLa, MCF7 and hippocampal neurons

(a) Corresponding fluorescence image of ATTO740-labeled 5-Ethynyl-2′-deoxyuridine (EdU) for newly synthesized DNA in the same cells as in Fig. 1c. (b) Representative epr-SRS images of ATTO740-labeled EdU through continuous 100 frame imaging. Frame numbers are indicated. Signal intensity curves are shown for imaging through 100 frames. The average photobleaching constant is determined to be 0.0003. (c) Epr-SRS imaging of ATTO740 immuno-labeled Giantin (Golgi membrane marker), Fibrillarin (nucleolar marker) in HeLa cells; alpha-tubulin and Neurofilament (Heavy, Neuronal Marker) in hippocampal neurons; and ATTO740 conjugated Wheat Germ Agglutinin (WGA), binded to membrane glycoproteins in live HeLa cells. (d) Epr-SRS imaging of ATTO740 immuno-labeled circulating tumor cell markers[35]: epithelial cell adhesion molecule (EpCAM); insulin-like growth factor 1 (IGF1) and CD44. Scale bar: 10 μm.

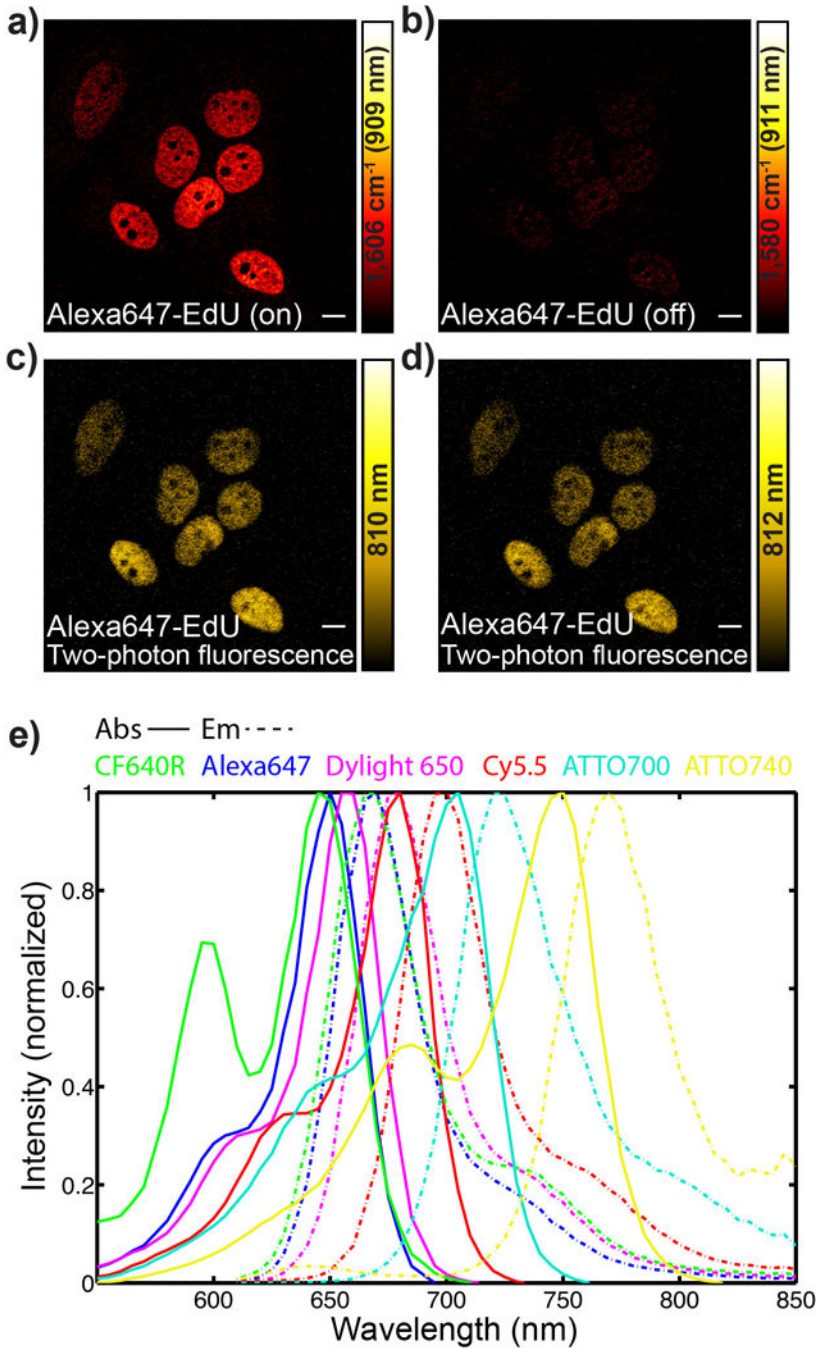

Extended Data Fig. 3. Chemical specificity comparison between Epr-SRS and fluorescence imaging

(a) On-resonance epr-SRS imaging of Alexa647 labeled EdU in HeLa cells at 1606 cm^{-1} (λ_{pump} = 909 nm). (b) Off-resonance image at 1580 cm^{-1} (λ_{pump} = 911 nm) of the same HeLa cells as in (a). (c-d) Two-photon fluorescence images of the same HeLa cells as in (a) at 810 nm (c) and 812 nm (d) around the two-photon excitation peak of Alexa647. (e) Absorption (solid) and emission (dashed) spectra for CF640R (green), Alexa647 (blue), DyLight650 (magenta), Cy5.5 (red), ATTO700 (cyan) and ATTO740 (yellow). Scale bar: 10 μm.

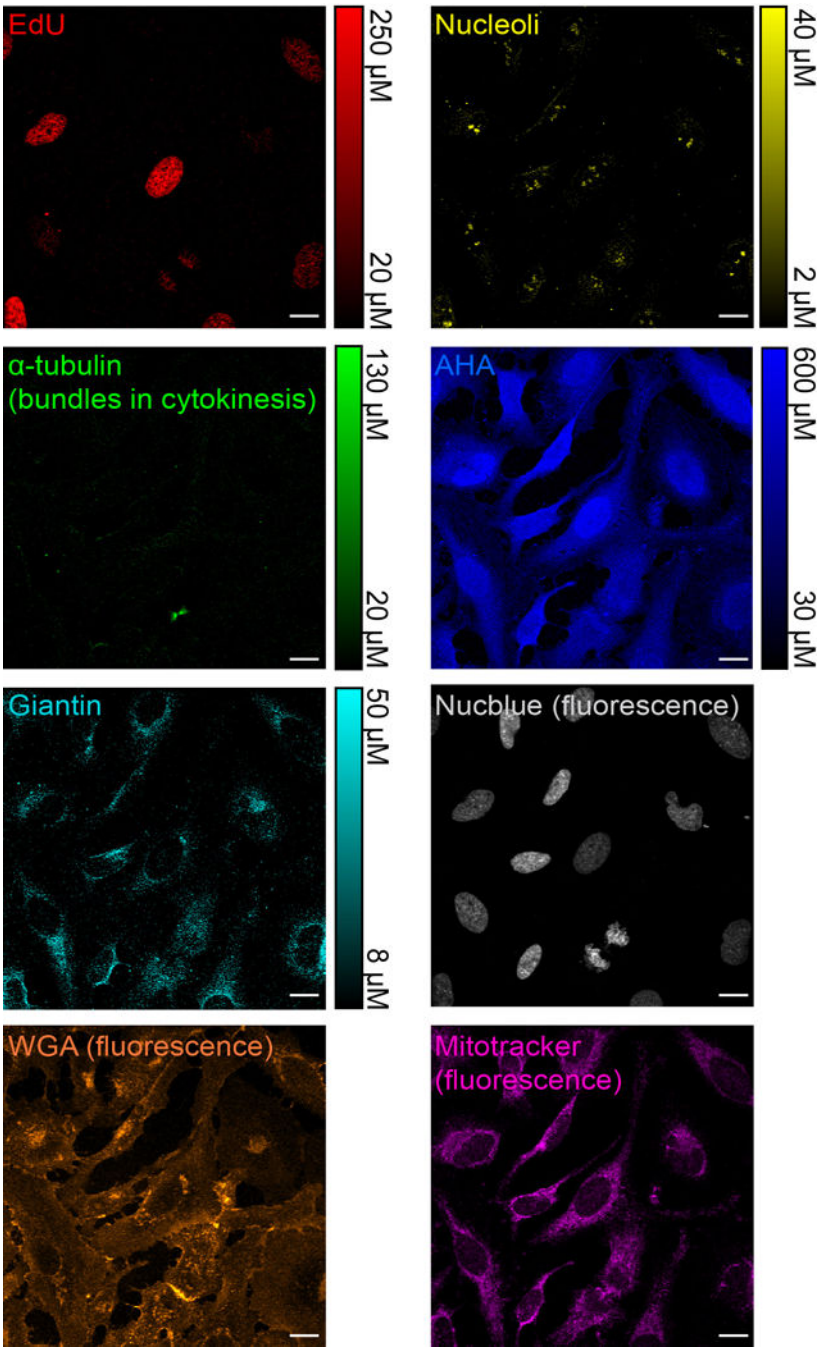

Extended Data Fig. 4. Quantitative epr-SRS and fluorescence imaging of non-overlaid images of Fig. 2c

Scale bar: 10 μm.

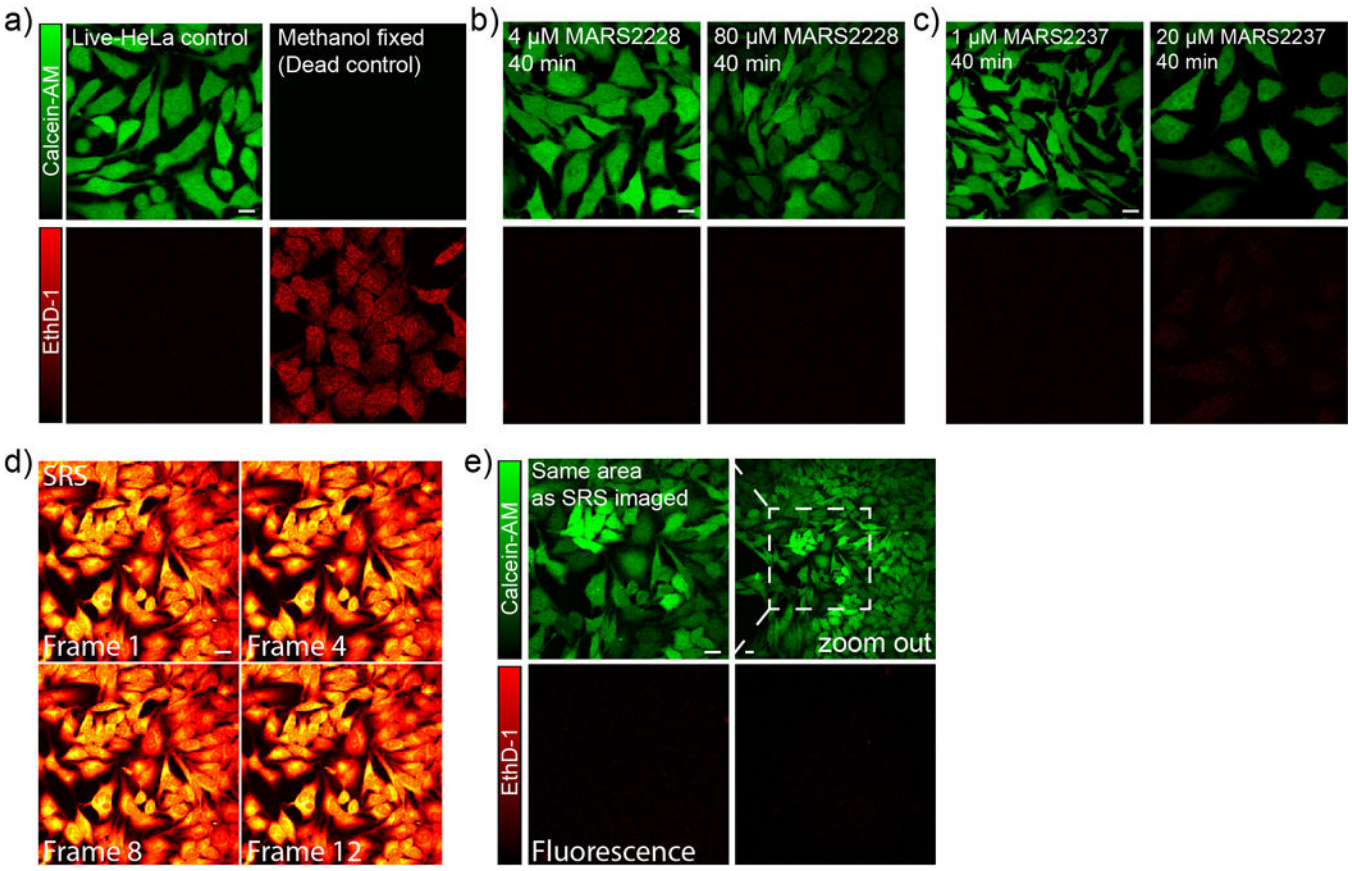

Extended Data Fig. 5. Minimum chemical-toxicity of MARS dyes for multicolor live-cell imaging (a-c) and photo-toxicity of SRS lasers (d-e)

(a) Control fluorescence images for live/dead cell viability assay for live HeLa cells (Calcein-AM, green, as live cell indicator) and fixed cells (EthD-1, red, as dead cell indicator). (b) Live/dead cell viability assay with 4 μM and 80 μM MARS2228 stained live cells did not reveal significant chemical toxicity and cell death. 4 μM concentration is the same as used for live-cell stains in Fig. 4a; and 80 μM with 20× concentration mimics the 20-color staining conditions. This test would lead to same results for MARS2200, MARS2176, MARS2147 due to the minimum chemical structural changes by isotopic editing. (c) Similar live/dead cell viability assay with 1× and 20× concentration stain by MARS2237. This test would lead to same results for MARS2209, MARS2183, MARS2154. (d) 12 continuous frames of SRS imaging targeting vibrational peak of CH_3 (2940 cm^{-1}) with the same laser power and dwell time used for multiplex live-cell imaging. (e) Fluorescence image of the same set of pre-imaged cells in (d) with live/dead cell viability assay did not show observable cell death or any cell viability loss when compared to the surrounding cells without pre-exposure to the SRS laser. Scale bar: 10 μm.

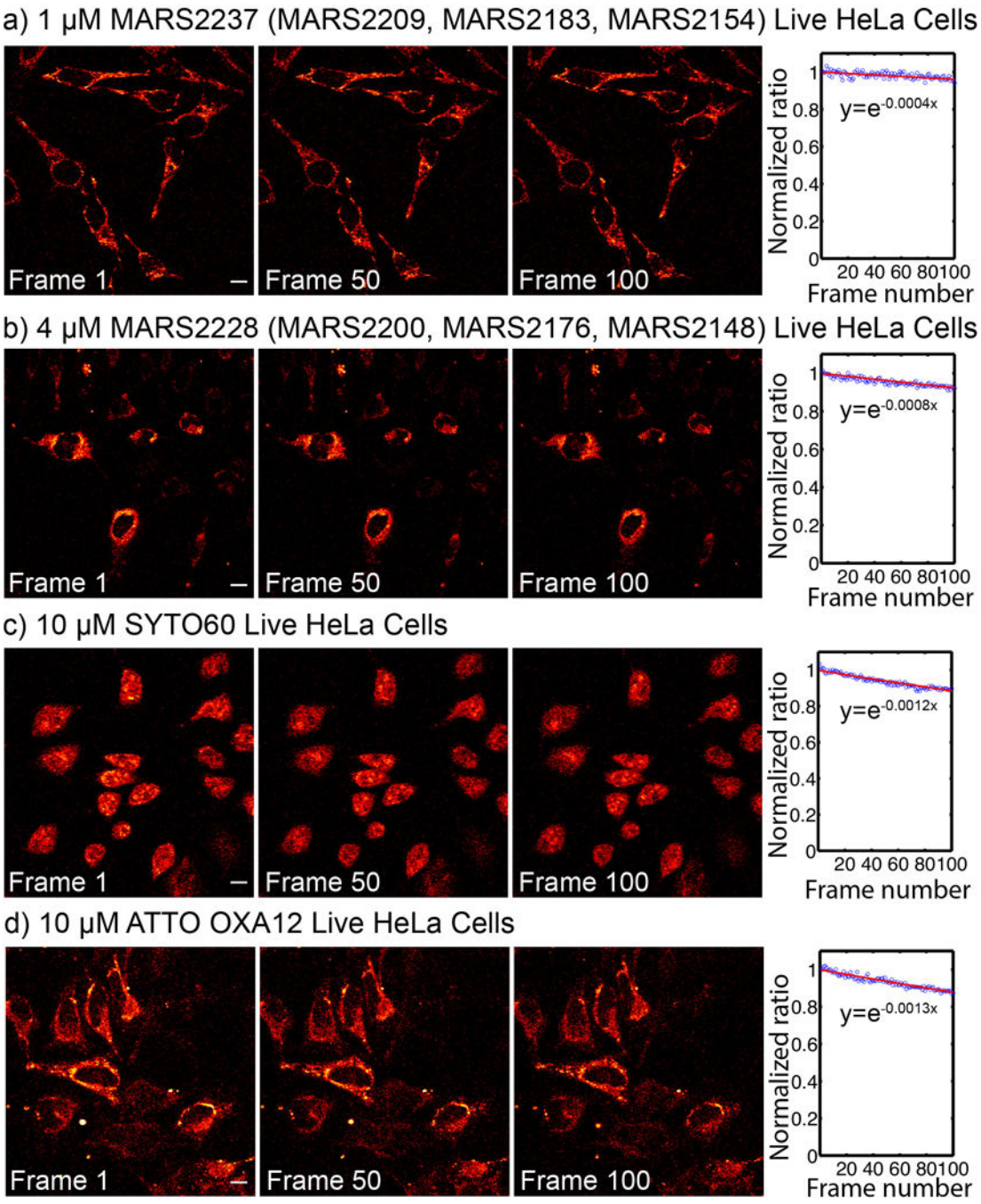

Extended Data Fig. 6. Photo-stability characterization for 10 representative epr-SRS dyes (including 8 MARS dyes) for live-cell imaging

The photobleaching percentage after 100 frames of SRS scans ranges from 4% to below 13%. Scale bar: 10 μm.

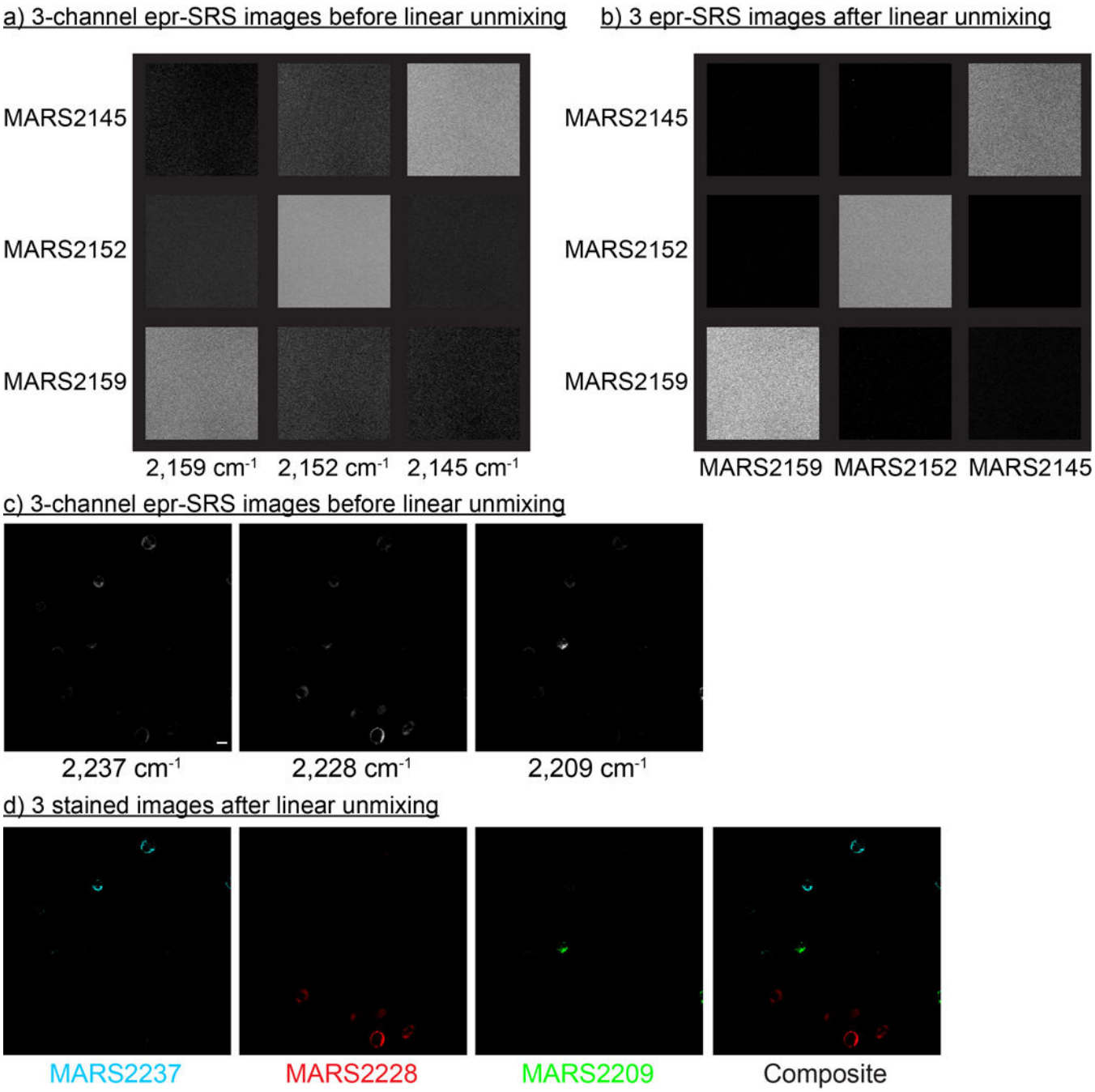

Extended Data Fig. 7. Linear unmixing on MARS solutions (a-b) and MARS dye stained cells (c-d)

(a) 3-channel epr-SRS images at 2159 cm^{-1}, 2152 cm^{-1}, 2145 cm^{-1} for 100 μM MARS2145; 1000 μM MARS2152, 300 μM MARS2159 before unmixing. (b) Images after linear unmixing with average readings of 94, 1097 and 315 in the unit of μM for MARS2145, MARS2152 and MARS2159. (c) Raw epr-SRS images for 3-color cell-mix after each stained with 1 μM MARS2237, 4 μM MARS2228, 1 μM MARS2209 separately before linear unmixing. (d) Images and their composite after linear unmixing.

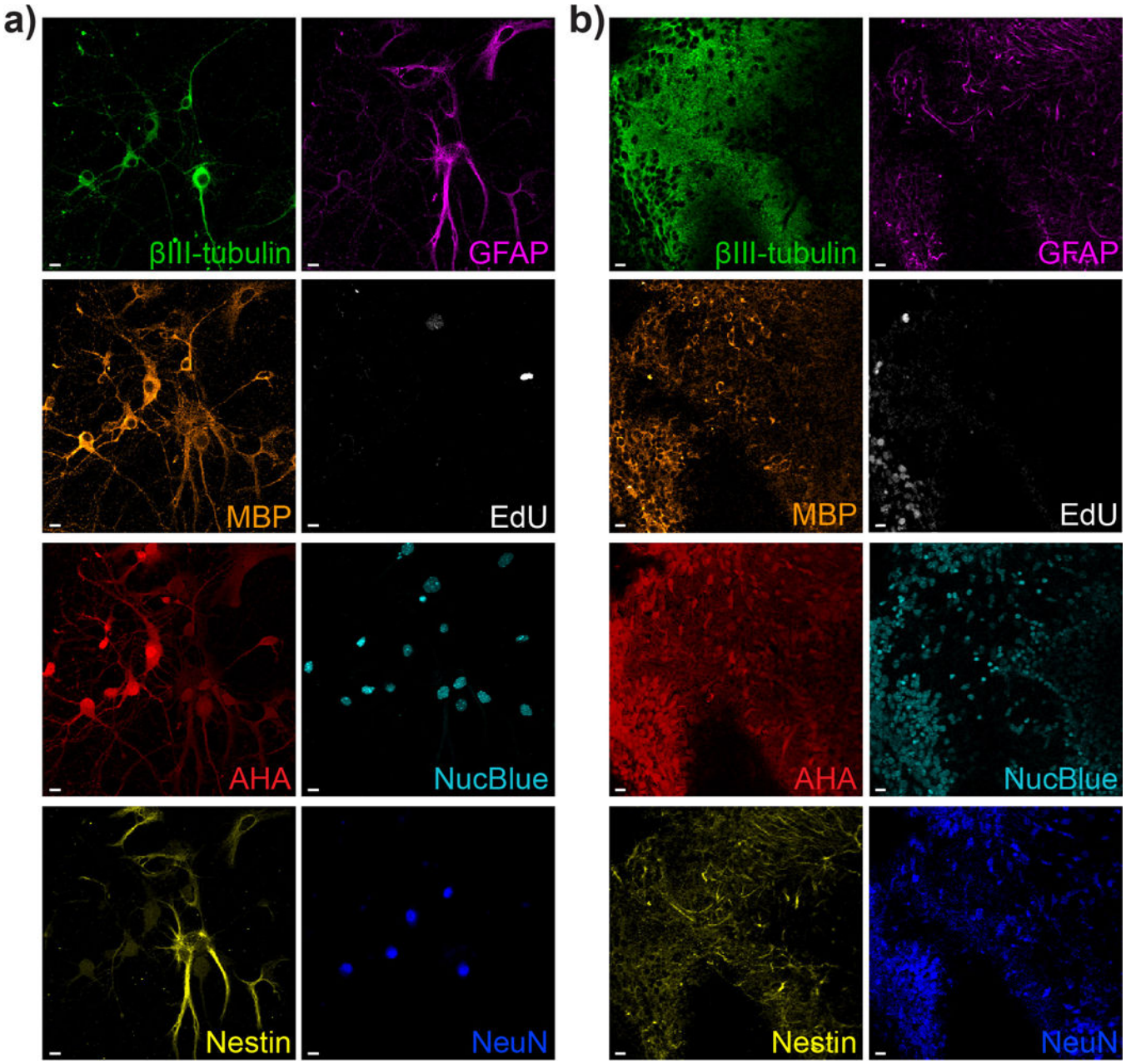

Extended Data Fig 8.

8-color epr-SRS and fluorescence imaging of non-overlaid images of (a) hippocampal neuronal cultures in Fig. 4b; (b) Organotypic cerebellar brain slices in Fig. 4c. Scale bar: 10 μm.

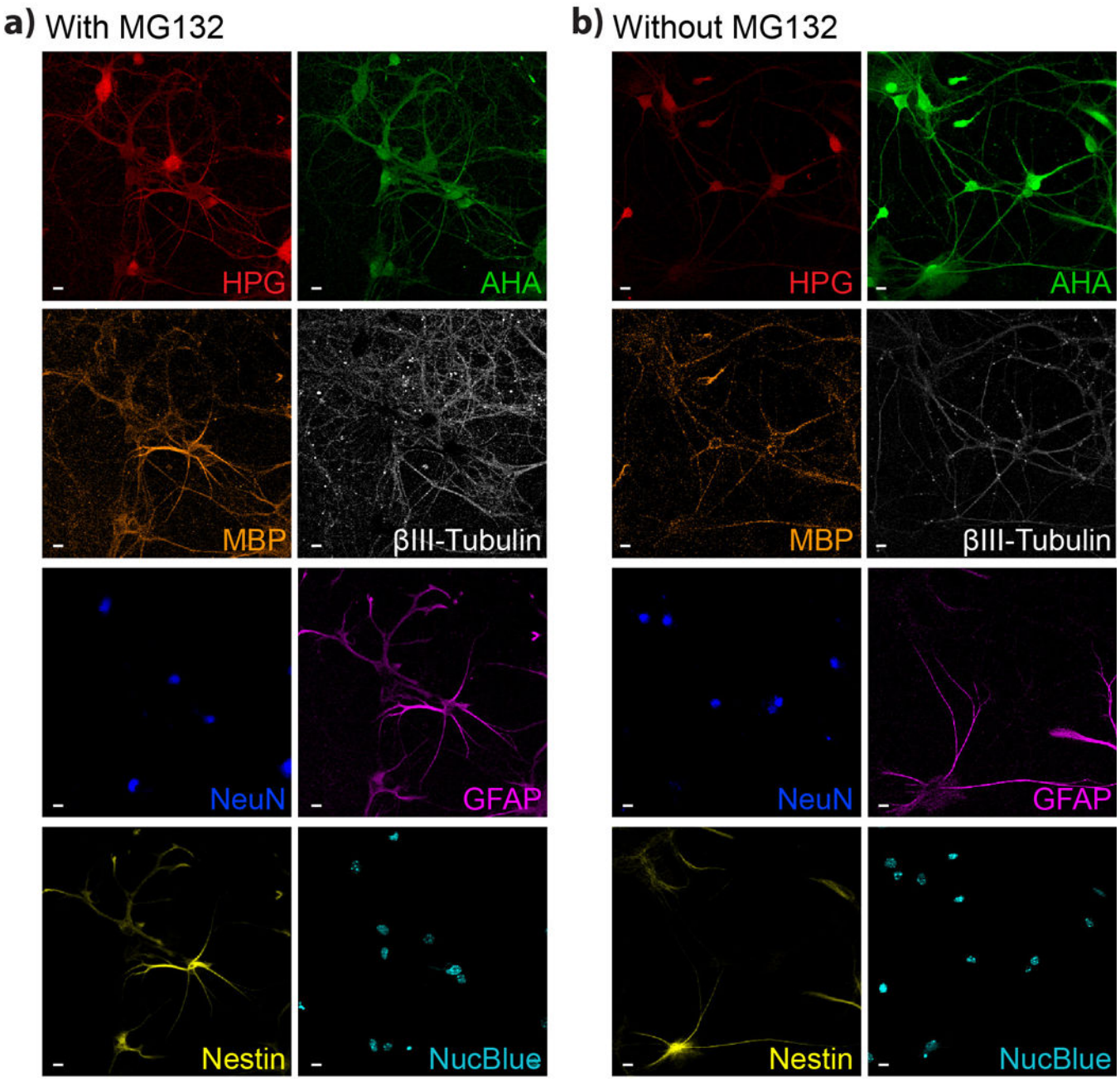

Extended Data Fig. 9.

8-color epr-SRS and fluorescence imaging of non-overlaid images of (a) hippocampal neuronal cultures treated with MG132 as in Fig. 4d. (b) Control set without MG132 treatment. Scale bar: 10 μm.

Extended Data Table 1

Raman cross-sections of 28 commercial dyes with molecular absorption peaks across a large energy range

The absolute Raman cross-section for C-O in methanol is 2.1×10^{-30} cm^2 at 785 nm [36], and extrapolated to 0.9×10^{-30} cm^2 under our pump wavelength. Raman cross-sections are listed in reference to C-O Raman cross-section in methanol. Solvent: a: Water; b: DMSO; c: Methanol; d: Water +5% DMSO; e: 50% Water + 50% DMSO.

Name	Commercial source	λ_{max} (nm)	Double bond Raman Peak (cm^{-1})	Raman cross section (cm^2)*	S/B ratio	Solvent
Benzotriazole	B11400, Sigma	262	1,394	8.1×10^{-30}	20	a
Coumarin 153	546186, Sigma	430	1,604	2.1×10^{-28}	6	b
Rhodamine 6G	83697, Sigma	532	1,656	6.8×10^{-28}	40	a
Rhodamine B	83689, Sigma	558	1,659	1.1×10^{-27}	15	a
Sulforhodamine 101	S7635, Sigma	590	1,659	2.4×10^{-27}	60	d
Alexa633	A20105, Invitrogen	630	1,653	8.4×10^{-27}	19	d
Mitotracker deep red FM	M22426, Invitrogen	645	1,604	1.3×10^{-26}	5	e
CF640R	92085, Biotium	647	1,665	1.4×10^{-26}	10	d
Alexa647	A10277, Invitrogen	651	1,606	0.9×10^{-26}	2.5	d
Cy5	777323, Sigma	654	1,606	1.7×10^{-26}	4	d
DyLight650	62265, Thermo Scientific	658	1,606	1.0×10^{-26}	2.6	d
ATTO655	11774 Sigma	665	1,665	1.8×10^{-26}	10	d
Cyanine5.5	178, AAT-Bioquest	680	1,626	1.3×10^{-26}	2.2	d
Alexa680	A20008, Invitrogen	682	1,629	1.2×10^{-26}	1	d
ATTO-Oxa12	55785 SIGMA	682	1,659	2.3×10^{-26}	3.5	b
ATTO665	04022 SIGMA	682	1,641	2.3×10^{-26}	60	b
ATTO680	94875 Sigma	686	1,662	2.2×10^{-26}	75	b
Methylene Blue	M9140 Stoma	688	1,630	2.1×10^{-26}	21	b
Rhodamine800	83701 Sigma	700	1,652	2.9×10^{-26}	84	b
ATTO700	30674, Sigma	708	1,657	3.3×10^{-26}	40	b
Alexa700	A20010, Invitrogen	718	1,625	1.6×10^{-26}	1.8	b
ATTO725	47156 Sigma	744	1,640	7.8×10^{-26}	78	b
ATTO740	91394 Sigma	760	1,642	1.4×10^{-25}	80	b
3.3′-Diethylthiatricar bocyanine iodide	381306 Sigma	762	1,671	1.4×10^{-25}	5	c
Alexa750	A20011, Invitrogen	772	1,604	0.6×10^{-25}	1.4	b
Sulfo-Cyamine7	15320, Lumiprobe	774	1,622	1.5×10^{-25}	1.5	b
Cyamine7.5	A6030, Lumiprobe	800	1,628	1.9×10^{-25}	0.5	b
IR820	543365 Sigma	840	1,628	5.8×10^{-25}	0.3	b

Extended Data Table 2
Raman cross-sections of 22 MARS dyes

The absolute Raman cross-section for C-O in methanol is 2.1×10^{-30} cm^2 at 785 nm [36], and extrapolated to 0.9×10^{-30} cm^2 under our pump wavelength. Raman cross-sections are listed in reference to C-O Raman cross-section in methanol.

Name	λ_{max} (nm)	Triple bond Raman Peak (cm^{-1})	Raman cross section (cm^2)*	S/B ratio	Solvent
MARS2228	760	2,228	9.2×10^{-26}	12	DMSO
MARS2200	760	2,200	9.2×10^{-26}	8.8	DMSO
MARS2176	760	2,176	9.2×10^{-26}	11.2	DMSO
MARS2147	760	2,147	9.2×10^{-26}	9.5	DMSO
MARS2225	760	2,225	6.4×10^{-26}	10.5	DMSO
MARS2199	760	2,199	6.4×10^{-26}	10	DMSO
MARS2173	760	2,173	6.4×10^{-26}	8.5	DMSO
MARS2145	760	2,145	6.4×10^{-26}	10	DMSO
MARS2233	735	2,233	2.1×10^{-26}	30	DMSO
MARS2204	735	2,204	2.1×10^{-26}	33	DMSO
MARS2179	735	2,179	2.1×10^{-26}	38	DMSO
MARS2152	735	2,152	2.1×10^{-26}	42	DMSO
MARS2101	720	2,101	3.0×10^{-26}	5.5	AcOH
MARS2061	720	2,061	2.8×10^{-26}	6.5	AcOH
MARS2237	700	2,237	2.4×10^{-26}	62	DMSO
MARS2209	700	2,209	2.4×10^{-26}	70	DMSO
MARS2183	700	2,183	2.4×10^{-26}	80	DMSO
MARS2154	700	2,154	2.4×10^{-26}	60	DMSO
MARS2242	667	2,242	1.5×10^{-26}	8	DMSO
MARS2214	667	2,214	1.5×10^{-26}	9.2	DMSO
MARS2186	667	2,186	1.5×10^{-26}	8	DMSO
MARS2159	667	2,159	1.5×10^{-26}	9	DMSO

Supplementary Material

Refer to Web version on PubMed Central for supplementary material.

Acknowledgments

We thank L. Brus and A. McDermott for stimulating discussions; M. Jimenez and C. Dupre for helpful suggestions, L. Shi for technical assistance. W. M. acknowledges support from NIH Director's New Innovator Award (1DP2EB016573), R01 (EB020892), the US Army Research Office (W911NF-12-1-0594), the Alfred P. Sloan Foundation and the Camille and Henry Dreyfus Foundation. R.Y. is supported by the NEI (EY024503, EY011787) and NIMH (MH101218, MH100561).

References

1. Lichtman JW, Denk W. The big and the small: challenges of imaging the brain's circuits. Science. 2011; 334:618–623. [PubMed: 22053041]
2. Chen KH, Boettiger AN, Moffitt JR, Wang S, Zhuang X. Spatially resolved, highly multiplexed RNA profiling in single cells. Science. 2015; 348:6233.
3. Giesen C, et al. Highly multiplexed imaging of tumor tissues with subcellular resolution by mass cytometry. Nat Methods. 2014; 11:417–422. [PubMed: 24584193]
4. Shroff H, et al. Dual-color superresolution imaging of genetically expressed probes within individual adhesion complexes. Proc Natl Acad Sci USA. 2007; 104:20308–20313. [PubMed: 18077327]
5. Lakowicz, JR. Principles of Fluorescence Spectroscopy. 3rd. Springer; 2011.
6. Dean KM, Palmer AE. Advances in fluorescence labeling strategies for dynamic cellular imaging. Nat Chem Biol. 2014; 10:512–523. [PubMed: 24937069]
7. Tsurui H, et al. Seven-color fluorescence imaging of tissue samples based on fourier spectroscopy and singular value decomposition. J Histochem Cytochem. 2000; 48:653–662. [PubMed: 10769049]
8. Niehörster T, et al. Multi-target spectrally resolved fluorescence lifetime imaging microscopy. Nat Methods. 2016; 13:257–262. [PubMed: 26808668]
9. Lane LA, Qian X, Nie S. SERS nanoparticles in medicine: from label-free detection to spectroscopic tagging. Chem Rev. 2015; 115:10489–10529. [PubMed: 26313254]
10. Min W, Freudiger CW, Lu S, Xie XS. Coherent nonlinear optical imaging: beyond fluorescence microscopy. Annu Rev Phys Chem. 2011; 62:507–530. [PubMed: 21453061]
11. Cheng J-X, Xie XS. Vibrational spectroscopic imaging of living systems: emerging platform for biology and medicine. Science. 2015; 350:aaa8870. [PubMed: 26612955]
12. Wei L, et al. Live-cell imaging of alkyne-tagged small biomolecules by stimulated Raman scattering. Nat Methods. 2014; 11:410–412. [PubMed: 24584195]
13. Hong S, et al. Live-cell stimulated Raman scattering imaging of alkyne-tagged biomolecules. Angew Chem Int Ed Engl. 2014; 53:5827–5831. [PubMed: 24753329]
14. Yamakoshi H, et al. Imaging of EdU, an alkyne-tagged cell proliferation probe, by Raman microscopy. J Am Chem Soc. 2011; 133:6102–6105. [PubMed: 21443184]
15. Weeks T, Wachsmann-Hogiu S, Huser T. Raman microscopy based on doubly-resonant four-wave mixing (DR-FWM). Opt Express. 2009; 17:17044–17051. [PubMed: 19770922]
16. Asher SA. UV Resonance Raman studies of molecular structure and dynamics: applications in physical and biophysical chemistry. Annu Rev Phys Chem. 1988; 39:537–588. [PubMed: 3075468]
17. McCamant DW, Kukura P, Mathies P. Femtosecond broadband stimulated Raman: a new approach for high-performance vibrational spectroscopy. Appl Spectrosc. 2003; 57:1317–1323. [PubMed: 14658143]
18. Le Ru EC, Etchegoin PG. Single-molecule surface-enhanced Raman spectroscopy. Annu Rev Phys Chem. 2012; 63:65–87. [PubMed: 22224704]
19. Albrecht AC, Hutley MC. On the dependence of vibrational Raman intensity on the wavelength of incident light. J Chem Phys. 1971; 55:4438–4443.
20. Yamakoshi H, et al. Alkyne-tag Raman imaging for visualization of mobile small molecules in live cells. J Am Chem Soc. 2012; 134:20681–20689. [PubMed: 23198907]
21. Shi J, Zhang X-P, Neckers DC. Xanthenes: Flourone Derivatives II. Tet Lett. 1993; 34:6013–6016.
22. Pastierik T, Šebej P, Medalová J, Štacko P, Klán P. Near-infrared fluorescent 9-phenylethynylpyronin analogues for bioimaging. J Org Chem. 2014; 79:3374–3382. [PubMed: 24684518]
23. Koide Y, et al. Development of NIR fluorescent dyes based on Si-Rhodamine for in vivo imaging. J Am Chem Soc. 2012; 134:5029–5031. [PubMed: 22390359]
24. Chen Z, et al. Multicolor live-cell chemical imaging by isotopically edited alkyne vibrational palette. J Am Chem Soc. 2014; 136:8027–8033. [PubMed: 24849912]

25. Kaushik S, Cuervo AM. Proteostasis and aging. Nat Med. 2015; 21:1406–1415. [PubMed: 26646497]
26. Jänen SB, Chaachouay H, Richter-Landsberg C. Autophagy is activated by proteasomal inhibition and involved in aggresome clearance in cultured astrocytes. Glia. 2010; 58:1766–1774. [PubMed: 20645412]
27. Goldberg AL. Protein degradation and protection against misfolded or damaged proteins. Nature. 2003; 426:895–899. [PubMed: 14685250]
28. Chen B, Retzlaff M, Roos T, Frydman J. Cellular strategies of protein quality control. Cold Spring Harb Perspect Biol. 2011; 3:a004374. [PubMed: 21746797]
29. Shu X, et al. Mammalian expression of infrared fluorescent proteins engineered from a bacterial phytochrome. Science. 2009; 324:804–807. [PubMed: 19423828]
30. Liao C-S, et al. Spectrometer-free vibrational imaging by retrieving stimulated Raman signal from highly scattered photons. Sci Adv. 2015; 1:e1500738. [PubMed: 26601311]

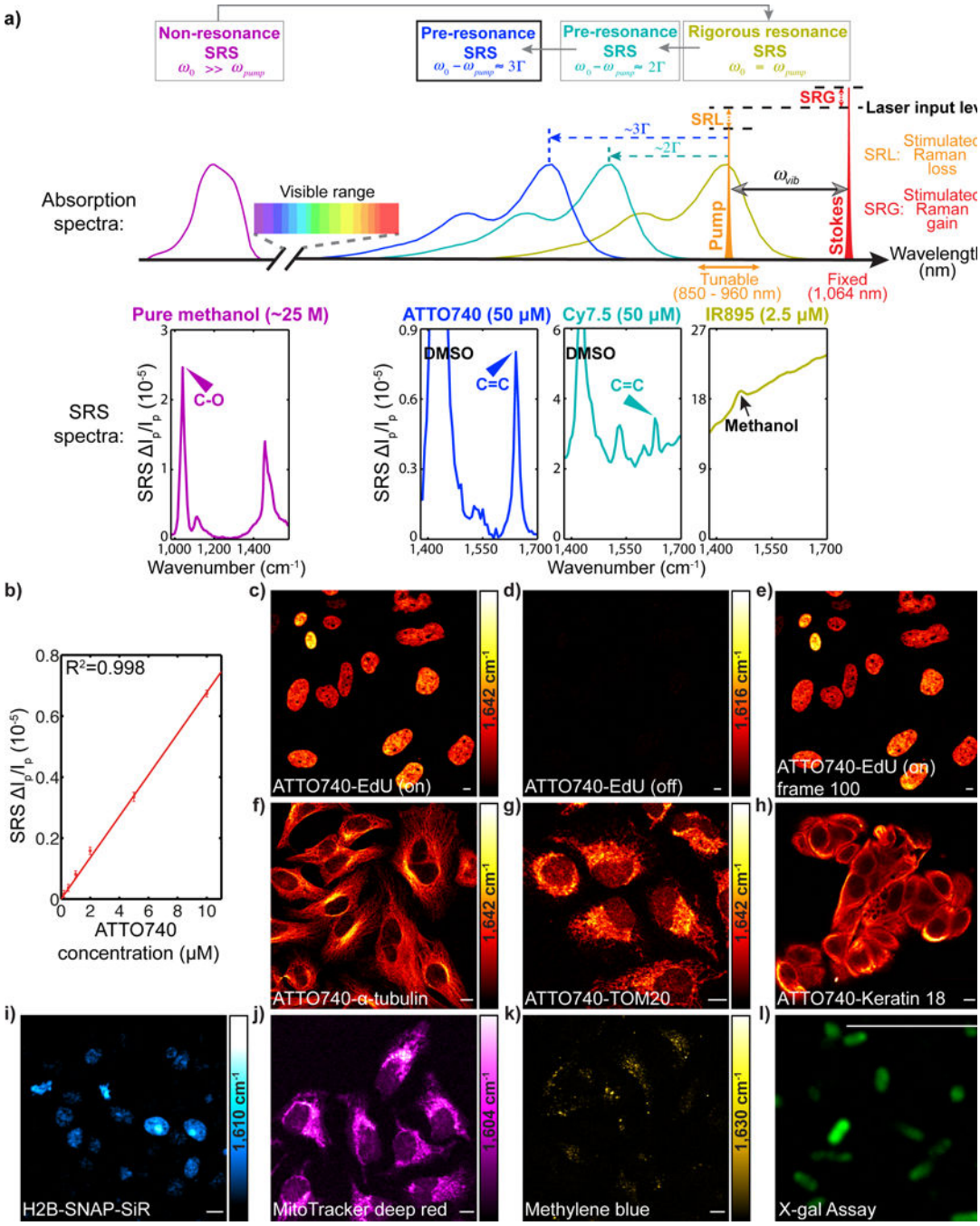

Fig. 1. Electronic pre-resonance stimulated Raman scattering (epr-SRS) microscopy

(a) Spectroscopy of different SRS regimes, defined by the energy difference between molecular absorption peak (ω_0) and pump laser (ω_{pump}). Representative SRS spectra at each regime: pure methanol at non-resonance; IR895 at rigorous resonance (λ_{abs} ~ 900 nm, methanol); Cy7.5 at pre-resonance (λ_{abs} ~ 800 nm, DMSO); ATTO740 at pre-resonance (λ_{abs} ~ 760 nm, DMSO). C-O band in non-resonance and C=C bands in pre-resonance are arrow-headed. Solvent bands are marked. Γ is the homogeneous linewidth, ~ 700 cm^{-1}. (b) Linear dependence of epr-SRS signals on ATTO740 concentrations (C=C at 1642 cm^{-1})

under a 1-ms time constant. (c) Fast epr-SRS imaging of ATTO740 click-labeled 5-Ethynyl-2'-deoxyuridine (EdU) for newly synthesized DNA in HeLa cells. (d) Off-resonance image and (e) The 100th frame image for the same set of cells shown in (c). (f-l) Epr-SRS imaging of ATTO740 immuno-labeled α-tubulin (f), Tom20 (g) in HeLa cells and Keratin 18 (h) in MCF7 cells; SiR SNAP-tagged genetically encoded H2B proteins (i), MitoTracker deep red (j), methylene blue (k) in live HeLa cells; and oxidation product 4,4'-dichloro-5,5'-dibromoindigo from X-gal hydrolysis in *E. coli* (l). Scale bar: 10 μm.

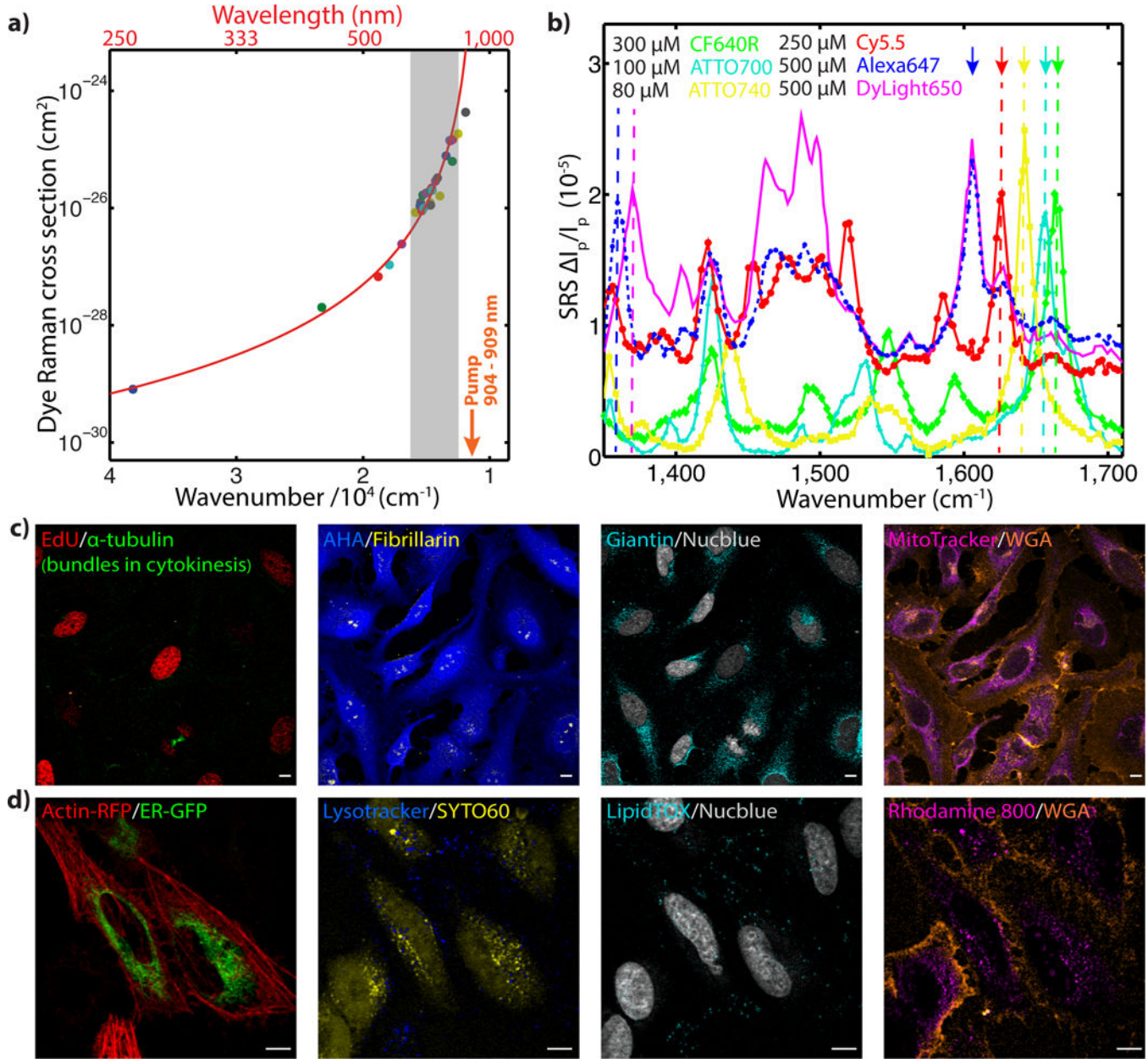

Fig. 2. Multiplex epr-SRS imaging with commercial dyes in fixed and live mammalian cells

(a) Semi-log plot of the measured Raman cross-sections for conjugated C=C of 28 organic dyes across a wide range of absorption peak energies (excited by λ_{pump} = 904 – 909nm). Grey-shaded area indicates the defined epr-SRS region. (b) Resolvable epr-SRS spectra of 6 commercial dyes (dash-lined): CF640R (1665 cm^{-1}), ATTO700 (1657 cm^{-1}), ATTO740 (1642 cm^{-1}), Cy5.5 (1626 cm^{-1}), Alexa647 (1606 cm^{-1}, 1359 cm^{-1}) and DyLight650 (1606 cm^{-1}, 1370 cm^{-1}). Occasional residual backgrounds (e.g. DyLight650) are likely from two-photon absorption. (c) 8-color epr-SRS (channels arrowed in b) and fluorescence imaging in fixed HeLa cells. Epr-SRS: EdU (newly synthesized DNA, Cy5.5, red), α-tubulin (bundles in cytokinesis, CF640R, green), Azidohomoalaine (AHA) (newly synthesized proteins, Alexa647, blue), Fibrillarin (nucleoli marker, ATTO740, yellow), Giantin (Golgi marker,

ATTO700, cyan). Fluorescence: Nucblue (total DNA, gray), Wheat Germ Agglutinin (WGA) (Glycoproteins, Alexa488, orange); MitoTracker orange (mitochondria marker, magenta). (d) 8-color imaging in live Hela cells. Epr-SRS: Lysotracker (lysosome marker, blue), SYTO60 (nucleic acid stain, yellow), LipidTOX Deep Red (neutral lipid stain, cyan), WGA (Glycoproteins, ATTO740, orange), Rhodamine 800 (mitochondria marker, magenta). Fluorescence: Actin (RFP, red), endoplasmic reticulum (ER) (GFP, green), Nucblue (total DNA, gray). Scale bar: 10 μm.

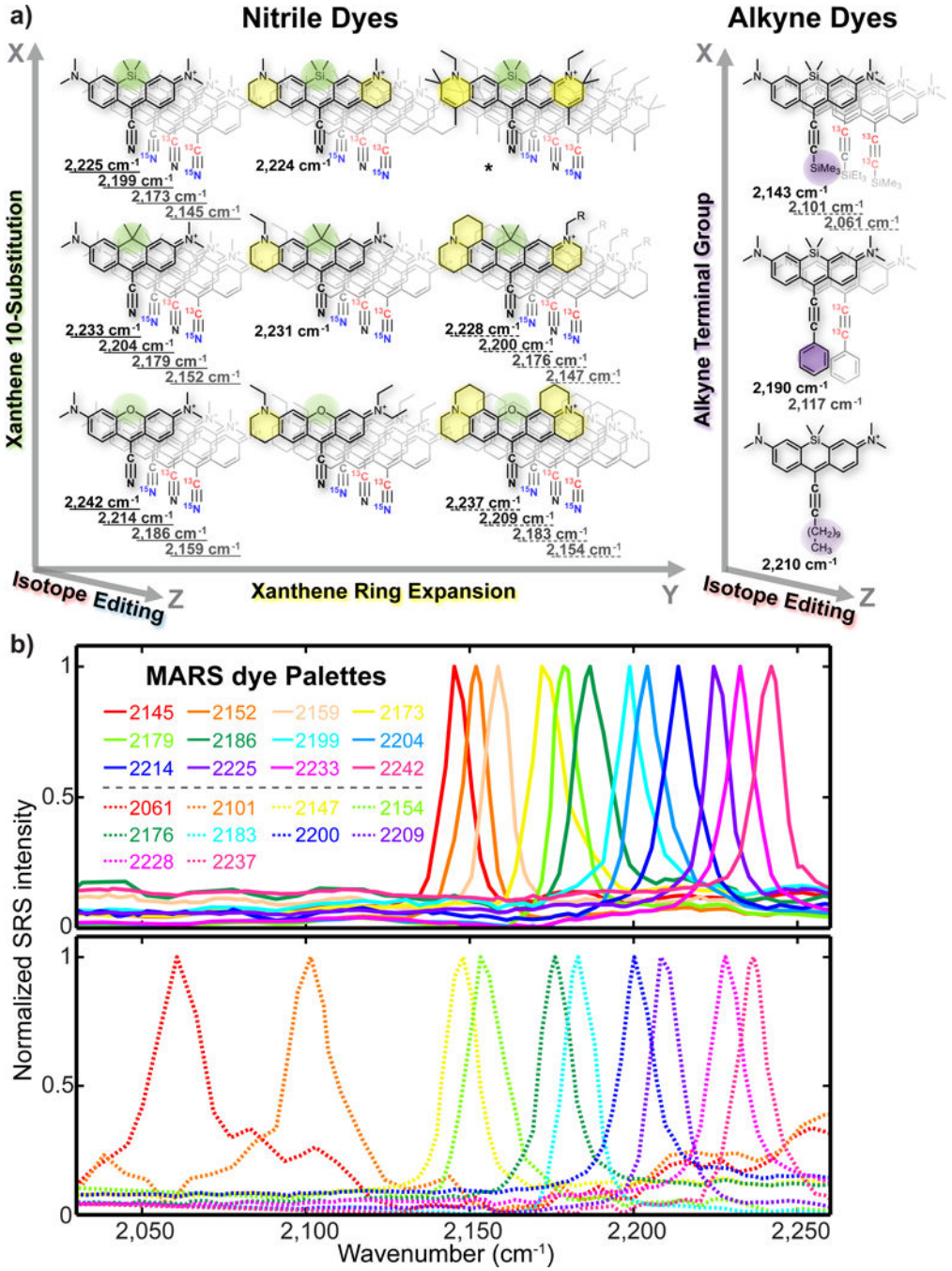

Fig 3. MAnhattan Raman Scattering (MARS) dyes bearing π-conjugated, isotopically-edited and electronically fine-tuned triple bonds

(a) Design principles and structures for a library of epr-SRS nitrile and alkyne dyes. *Overwhelming background due to close electronic resonance. (b) Two sets of MARS palettes and their normalized epr-SRS spectra in the cell-silent window. The upper panel contains 12 MARS dyes, whose vibrational frequencies are indicated by numbers after solid lines and the corresponding structures are solid-underlined in (a). The lower panel contains 10 MARS dyes, whose vibrational frequencies are indicated by numbers after dashed lines and the corresponding structures are dash-underlined in (a).

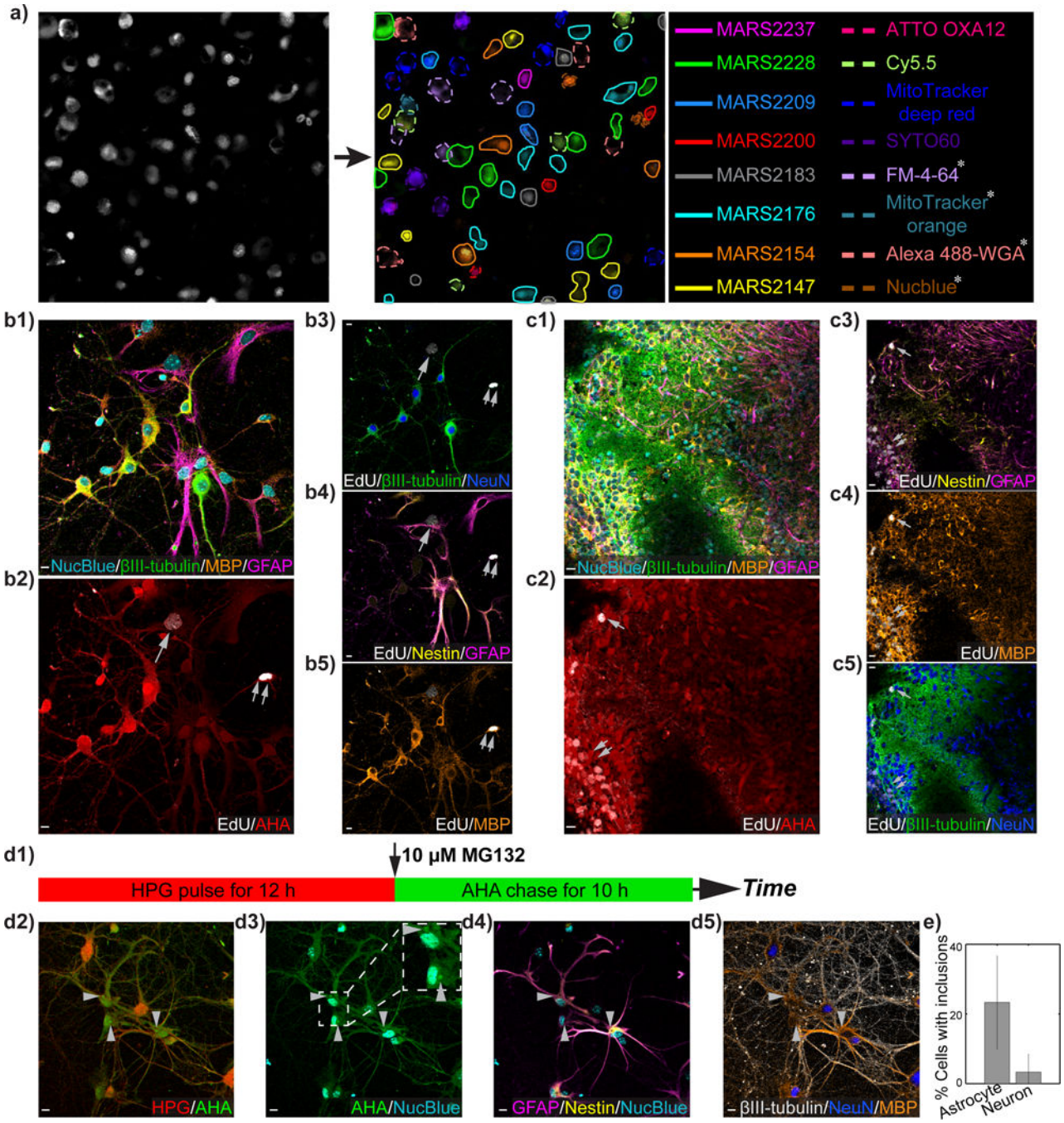

Fig. 4. Super-multiplex optical microscopy and its applications for probing metabolic activity in nervous systems under physiological and pathological conditions

(a) 16-color live-cell imaging with 8 MARS dyes, 4 commercial vibrational dyes in the fingerprint and 4 additional fluorescent dyes (star indicated). Each pre-stained cell in the cell mix (gray image, left) is circled with the matching line color and shape (16-color image, right) with the corresponding dye. (b-c) 8-color epr-SRS imaging of DNA replication and protein synthesis in hippocampal neuronal cultures (b1-b5) and organotypic cerebellar brain slices (c1-c5). (d1-d5) Pulse (HPG) – chase (AHA) imaging of proteome turnover dynamics in hippocampal neuronal cultures with proteasome inhibitor MG132 in the chase period,

with the percentages of astrocyte and neuron cells that contain protein inclusions shown in (e). Error bars, mean±s.d based on imaging n=6 samples (see also methods), with $P<0.01$ determined using two-sided Student's t-test. For labeling in b-c, Epr-SRS: βIII-tubulin (neurons, MARS2200, green in b-c; gray in d), Myelin basic protein (MBP) (oligodendrocytes, MARS2176, orange), Glial fibrillary acidic protein (GFAP) (astrocytes and neural stem cells, MARS2147, magenta), EdU (newly synthesized DNA, MARS2228, gray in b-c), HPG (proteins synthesized in pulse period, MARS2228, red in d), AHA (proteins synthesized in chase period, Alexa647, red in b-c; green in d). Fluorescence: Nucblue (total DNA, cyan), NeuN (neurons, Alexa568, blue), Nestin (neural stem cells and astrocytes, Alexa488, yellow). Scale bar: 10 μm.